Geophys. J. Int. (1998) **133,** 1–19

Postglacial sea-level change on a rotating Earth

Glenn A. Milne and Jerry X. Mitrovica

Department of Physics, University of Toronto, 60 *St. George Street, Toronto, Ontario, Canada,* M5S 1A7. *E-mail: milne@globe.physics.utoronto.ca*

Accepted 1997 September 24. Received 1997 September 11; in original form 1997 May 14

SUMMARY

We present a complete derivation of the equation governing long-term sea-level variations on a spherically symmetric, self-gravitating, Maxwell viscoelastic planet. This new 'sea-level equation' extends earlier work by incorporating, in a gravitationally self-consistent manner, both a time-dependent ocean–continent geometry and the influence of contemporaneous perturbations to the rotation vector of the planet. We also outline an efficient, pseudo-spectral, numerical methodology for the solution of this equation, and present a variety of predictions, based on a suite of earth models, of relative sea level (RSL) variations due to glacial isostatic adjustment (GIA). These results show that the contribution to the predicted RSL signal from GIA-induced perturbations to the rotation vector can reach 7–8 m over the postglacial period in geographic regions where the rotationally induced signal is a maximum. This result is sensitive to variations in the adopted lower-mantle viscosity and is relatively insensitive to variations in the adopted lithospheric thickness. We also show that the rotationally induced component of RSL change is sufficient to influence previous estimates of Late Holocene melting events and ongoing sea-level change due to GIA which were based on a RSL theory for a non-rotating Earth. In particular, estimates of Antarctic melting over the last 5 kyr, based on the amplitude of sea-level highstands from the Australian region, may require an adjustment downwards of the order of 0.5 m of equivalent sea-level rise. Furthermore, present-day rates of sea-level change are perturbed by as much as ~ 0.2 mm yr^{-1} by the rotational component of sea-level change, and this has implications for GIA corrections of the global tide gauge record. Over the period from the last glacial maximum to the present, we predict a distinctly non-monotonic variation in the rotation-induced component of RSL. This is in agreement with our previous preliminary study (Milne & Mitrovica 1996), but contrasts significantly with predictions presented by Han & Wahr (1989) and Bills & James (1996). We demonstrate that the disagreement arises as a consequence of approximations adopted in the latter studies. We furthermore refute an assertion by Bills & James (1996) that previously published constraints on mantle viscosity and ice-sheet histories which did not incorporate a rotation-induced RSL component are 'largely invalidated' by this omission.

Key words: Earth's rotation, glacial rebound, sea level.

1 INTRODUCTION

The last 20 kyr of Earth history has been characterized by a large and complex global signal of sea-level change. Many features of the spatial and temporal pattern of this signal are a result of the response of the Earth to the redistribution of ice and water masses occurring since the last glacial maximum (LGM). This climatically induced surface mass redistribution acts as an external load on the Earth which perturbs both the geoid and the solid surface, thus producing changes in sea level. A theory of load-induced postglacial sea-level change, culminating in the so-called 'sea-level equation', was first described by Farrell & Clark (1976). The Farrell & Clark (1976) theory has been used to predict many features of the global postglacial sea-level record (e.g. Farrell & Clark 1976; Peltier & Andrews 1976; Wu & Peltier 1983; Nakada & Lambeck 1989; Mitrovica & Peltier 1991; Lambeck 1993). For example, in the 'near field', the rebound of crustal regions once covered by the Late Pleistocene ice sheets causes a net sea-level fall as the upward movement of the solid surface dominates the eustatic sea-level rise associated with the influx of glacial meltwater to the oceans. Peripheral to these areas,

GJI000 24/3/98 10:30:44 3B2 version 5.20
The Charlesworth Group, Huddersfield 01484 517077

the collapse of the solid surface bulge contributes a sea-level rise which adds to the meltwater signal. In the 'far field' more subtle, second-order mechanisms such as continental levering (e.g. Clark, Farrell & Peltier 1978; Nakada & Lambeck 1989) and ocean syphoning (Mitrovica & Peltier 1991; Johnston 1993) become more evident, perturbing the dominant eustatic signal.

The surface mass redistribution and consequent Earth deformation also induces change in the Earth's rotation vector (e.g. Sabadini, Yuen & Boschi 1982; Wu & Peltier 1984). The corresponding change in the rotational potential deforms both the solid surface and the geoid, contributing a sea-level signal that is not incorporated into the sea-level theory of Farrell & Clark (1976). This rotation-induced signal arises primarily from the wander of the rotation pole relative to the surface geography (rather than from changes in the length of day), and hence is dominated by the geometry of the degree 2 order 1 spherical harmonic function (e.g. Han & Wahr 1989).

On timescales of 1–10 kyr and longer, perturbations to the rotation vector are associated with both glacial isostatic adjustment (GIA) and mantle convection (e.g. Spada, Ricard & Sabadini 1992; Steinberger & O'Connell 1997). In considering the influence of mantle-convection-induced polar wander on sea-level change, Sabadini, Doglioni & Yuen (1990) found that a uniform polar wander of 1° Myr^{-1} can produce a sea-level signal of up to 50 m when only the effect of rotational potential forcing is considered (that is, the loading effect produced by this sea-level change was not included). Perturbations to the rotation vector occurring over shorter timescales, for example the annual and Chandler wobbles, produce the well-studied sea-level phenomenon of pole tides (e.g. Miller & Wunsch 1973; Wahr 1985). Our interest here is the rotational signature induced by GIA and its corresponding influence on postglacial sea-level change. A number of studies have considered this topic (Han & Wahr 1989; Milne & Mitrovica 1996; Bills & James 1996); however, the results of these studies appear to be in significant disagreement.

Han & Wahr (1989) were the first to consider the effect of GIA-induced change in the rotation vector on sea level. Using a viscoelastic earth model with an isoviscous mantle of 10^{21} Pa s and a lithospheric thickness of 120 km, their results show that the predicted change in sea level may be described by a degree 2 order 1 spherical harmonic function with a maximum (peak to peak) signal of $\sim$28 m. Their predicted relative-sea-level (RSL) curves are characterized by a monotonic form with an amplitude variation of up to $\sim$14 m from 18 kyr BP to the present. In their analysis, Han & Wahr (1989) assumed a eustatic ocean load and modelled the Laurentide ice sheet using a single ice disc. Also, they did not consider the direct effect of the changing rotational potential on sea level. (We use the term 'direct' to denote the component of the sea-level response that is independent of Earth deformation for a specified surface load or potential forcing.) Milne & Mitrovica (1996) (hereafter referred to as MM) extended the study of Han & Wahr (1989) by using a more realistic global model of the late Pleistocene ice loading cycles and by computing a gravitationally self-consistent ocean load via the solution of a new sea-level equation valid for a rotating Earth. The results of MM differ markedly from those of Han & Wahr (1989). In particular, the predictions of MM are approximately half the amplitude and exhibit a significantly more complex temporal form than those of Han & Wahr (1989).

The most recent paper on the subject, by Bills & James (1996), has similarities to the analysis of Han & Wahr (1989) in that only the Laurentide ice mass and a eustatic ocean load are considered. Bills & James (1996) conclude that calculations based on a rigid earth model give a 'reasonable first order estimate of the polar motion contribution to relative sea level'. If this suggestion is correct, then the problem is greatly simplified because only the direct effect of the rotational potential needs to be considered (that is the sea-level response associated with the deformation induced by the changing rotational potential can be neglected). Using the rigid earth approximation, Bills & James (1996) predicted a rotation-induced postglacial sea-level signal that is of similar magnitude but of opposite sign to the prediction of Han & Wahr (1989).

In the following, we investigate these various discrepancies in more detail and show that the models of Han & Wahr (1989) and Bills & James (1996) lead to significant overestimates of the effect of GIA-induced polar wander on postglacial sea level. Our investigation also verifies the validity of the theory and results presented in MM.

A major purpose of the present article is to extend and complete the study of MM in several important aspects. MM focused on predicting present-day rates of sea-level change along the US east coast as a first application of their model. Using earth models characterized by a lithospheric thickness of 120 km and an upper-mantle viscosity of 10^{21} Pa s, MM found that the rotation-induced rate of sea-level change at Portland, ME ($\sim$0.12 mm yr^{-1}), was relatively insensitive to variations in lower-mantle viscosity in the range $3\text{–}50 \times 10^{21}$ Pa s. We extend this analysis by calculating the *global* signal of present-day sea-level-change rate for a range of lower-mantle viscosities and lithospheric thicknesses. MM also predicted RSL curves at two far-field sites located in regions where glaciation-induced polar wander produces a relatively large sea-level signal. These predictions were carried out using a single earth model (characterized by a lower-mantle viscosity of 5×10^{21} Pa s), and the resulting rotation effects were found to influence both the amplitude of the sea-level highstands at $\sim$5 kyr BP and the total sea-level change between LGM and the present. In this work we extend these calculations by considering a globally distributed set of sites and by investigating the sensitivity of our results to variations in the viscosity structure of the adopted earth model. Finally, MM presented only a cursory derivation of the sea-level equation valid for a rotating Earth. In the next section, we provide a complete derivation of this equation.

2 THEORY

We begin by reviewing the theory governing load-induced sea-level change on a non-rotating, spherically symmetric, self-gravitating, Maxwell viscoelastic earth model (Farrell & Clark 1976; Peltier & Andrews 1976). We then generalize this theory by deriving the sea-level equation valid for a rotating Earth. Finally, we outline how this extended sea-level equation can be solved numerically in a gravitationally self-consistent manner.

2.1 The sea-level equation for a non-rotating Earth

The theory of load-induced sea-level change that we adopt is based on the non-dimensional load Love numbers which

GJI000 24/3/98 10:31:17 3B2 version 5.20
The Charlesworth Group, Huddersfield 01484 517077

define the impulse response of a Maxwell viscoelastic earth model (Peltier 1974). In order to calculate the load-induced perturbations to the geoid and solid surface we require the so-called h and k surface load Love numbers which have the form (e.g. Peltier 1976)

$$h_\ell^{\mathrm{L}}(t) = h_\ell^{\mathrm{L,E}}\delta(t) + \sum_{k=1}^{K} r_k^{\ell,\mathrm{L}} \exp(-s_k^\ell t) \tag{1}$$

and

$$k_\ell^{\mathrm{L}}(t) = k_\ell^{\mathrm{L,E}}\delta(t) + \sum_{k=1}^{K} r_k'^{\ell,\mathrm{L}} \exp(-s_k^\ell t)\,, \tag{2}$$

where t is time, δ is the Dirac delta function and ℓ is the spherical harmonic degree. The superscript L is used to denote parameters associated with the surface mass loading problem. The first term on the right-hand side of each equation represents the immediate elastic response, while the second term describes the non-elastic response characterized by a set of K modes of exponential decay (note that the non-elastic response has a non-zero contribution at the instant the load is applied). Each mode is defined by an inverse decay time (s_k^ℓ) and amplitude ($r_k^{\ell,L}$ or $r_k'^{\ell,L}$), both of which depend on the viscoelastic profile of the adopted earth model. The Love numbers (1) and (2) can be used to construct impulse response Green's functions for the gravitational potential perturbation on the undeformed surface, and the radial displacement of the solid surface. These are, respectively (e.g. Mitrovica & Peltier 1991),

$$\Phi^{\mathrm{L}}(\gamma, t) = \frac{ag}{M_{\mathrm{e}}} \sum_{\ell=0}^{\infty} \left\{ \delta(t) + k_\ell^{\mathrm{L,E}}\delta(t) + \sum_{k=1}^{K} r_k'^{\ell,L} \exp(-s_k^\ell t) \right\} \times P_\ell(\cos\gamma) \tag{3}$$

and

$$\Gamma^{\mathrm{L}}(\gamma, t) = \frac{a}{M_{\mathrm{e}}} \sum_{\ell=0}^{\infty} \left\{ h_\ell^{\mathrm{L,E}}\delta(t) + \sum_{k=1}^{K} r_k^{\ell,L} \exp(-s_k^\ell t) \right\} P_\ell(\cos\gamma)\,, \tag{4}$$

where M_{e} is the mass of the Earth, a is the mean radius of the Earth, g is the surface gravitational acceleration and γ represents the angular distance between the impulse load point and the observation point. The first Dirac delta function on the right-hand side of eq. (3) denotes the direct effect of the impulse surface load on the Earth's gravitational potential. The P_ℓ are Legendre polynomials.

Let the general surface load, $L(\theta, \psi, t)$, where θ and ψ are the colatitude and east-longitude, respectively, represent a model of the spatio–temporal variation of the ice–ocean mass exchange. In this case, we can write

$$L(\theta, \psi, t) = \rho_{\mathrm{i}} I(\theta, \psi, t) + \rho_{\mathrm{w}} S(\theta, \psi, t)\,, \tag{5}$$

where ρ_{i} and ρ_{w} are, respectively, the densities of ice and water, and $I(\theta, \psi, t)$ and $S(\theta, \psi, t)$ are functions describing changes in ice and ocean thickness from the beginning of the loading period. The load-induced perturbations to the geoid and solid surface are calculated by convolving, in space and time, $L(\theta, \psi, t)$ with the Green's functions (3) and (4). The geoid anomaly, G^{L}, and the solid surface radial displacement, R^{L}, are given by

$$G^{\mathrm{L}}(\theta, \psi, t) = \frac{1}{g} \int_{-\infty}^{t} \iint_{\Omega} a^2 L(\theta', \psi', t') \Phi^{\mathrm{L}}(\gamma, t-t') d\Omega'\, dt' + \frac{\Delta\Phi^{\mathrm{L}}(t)}{g} \tag{6}$$

and

$$R^{\mathrm{L}}(\theta, \psi, t) = \int_{-\infty}^{t} \iint_{\Omega} a^2 L(\theta', \psi', t') \Gamma^{\mathrm{L}}(\gamma, t-t') d\Omega'\, dt'\,, \tag{7}$$

where Ω represents the complete solid angle and $[\Delta\Phi^{\mathrm{L}}(t)]/g$ is a globally uniform height shift of the geoid which is constrained by invoking surface load mass conservation. In deriving eq. (6) we have applied Bruns' formula (e.g. Heiskanen & Moritz 1967) to give a first-order determination of the radial warping of the geoid produced by a perturbation to the geopotential.

An expression for sea-level change is now obtained by taking the difference between the perturbed geoid and solid surface and multiplying by the time-dependent ocean function $C(\theta, \psi, t)$ (Munk & MacDonald 1960; the ocean function is defined to be unity over ocean regions and zero over land regions). Thus, we have

$$\begin{aligned} S(\theta, \psi, t) &= C(\theta, \psi, t)[G^{\mathrm{L}}(\theta, \psi, t) - R^{\mathrm{L}}(\theta, \psi, t)] \\ &= C(\theta, \psi, t) \left[\int_{-\infty}^{t} \iint_{\Omega} a^2 L(\theta', \psi', t') \right. \\ &\quad \left. \times \left\{ \frac{\Phi^{\mathrm{L}}(\gamma, t-t')}{g} - \Gamma^{\mathrm{L}}(\gamma, t-t') \right\} d\Omega'\, dt' + \frac{\Delta\Phi^{\mathrm{L}}(t)}{g} \right]. \end{aligned} \tag{8}$$

Eq. (8) is the sea-level equation for a Maxwell viscoelastic, non-rotating earth model. Since the sea-level change, $S(\theta, \psi, t)$, is required to define the loading function, $L(\theta, \psi, t)$ (see eq. 5), eq. (8) is an integral equation.

To solve the temporal convolution in (8) we model the time history of the load as a series of Heaviside loading increments (e.g. Farrell & Clark 1976; Peltier & Andrews 1976),

$$L(\theta, \psi, t) = \sum_{n=1}^{N} [\rho_{\mathrm{i}} \delta I^n(\theta, \psi) + \rho_{\mathrm{w}} \delta S^n(\theta, \psi)] H(t - t_n)\,. \tag{9}$$

Using (9) in eq. (8) and applying eq. (5) gives the result

$$\begin{aligned} &S(\theta, \psi, t) \\ &= C(\theta, \psi, t) \left[\iint_{\Omega} a^2 (\rho_{\mathrm{i}} I(\theta', \psi', t) + \rho_{\mathrm{w}} S(\theta', \psi', t)) Z^{\mathrm{L,E}}(\gamma) d\Omega' \right. \\ &\quad + \sum_{n=1}^{N} H(t - t_n) \iint_{\Omega} a^2 (\rho_{\mathrm{i}} \delta I^n(\theta', \psi') + \rho_{\mathrm{w}} \delta S^n(\theta', \psi')) \\ &\quad \left. \times Z^{\mathrm{L,NE}}(\gamma, t - t_n) d\Omega' + \frac{\Delta\Phi^{\mathrm{L}}(t)}{g} \right], \end{aligned} \tag{10}$$

where

$$Z^{\mathrm{L,E}}(\gamma) = \frac{a}{M_{\mathrm{e}}} \sum_{\ell=0}^{\infty} E_\ell^{\mathrm{L}} P_\ell(\cos\gamma)\,, \tag{11a}$$

$$Z^{\mathrm{L,NE}}(\gamma, t - t_n) = \frac{a}{M_{\mathrm{e}}} \sum_{\ell=0}^{\infty} \beta_\ell^{\mathrm{L}}(t - t_n) P_\ell(\cos\gamma)\,, \tag{11b}$$

GJI000 24/3/98 10:31:23 3B2 version 5.20
The Charlesworth Group, Huddersfield 01484 517077

with

$$E_\ell^{\mathrm{L}} = 1 + k_\ell^{\mathrm{L,E}} - h_\ell^{\mathrm{L,E}}, \tag{12a}$$

and

$$\beta_\ell^{\mathrm{L}}(t-t_n) = \sum_{k=1}^{K} \frac{(r_k'^{\ell,\mathrm{L}} - r_k^{\ell,\mathrm{L}})}{s_k^\ell} [1 - \exp(-s_k^\ell (t-t_n))]. \tag{12b}$$

The superscripts E and NE represent parameters associated with the elastic and non-elastic response, respectively.

The next step is to evaluate the spatial convolution in (10). This can be done by transforming the problem into the domain of spherical harmonics. Using the general spectral decomposition

$$\mathscr{X}(\theta, \psi) = \sum_{\ell,m} \mathscr{X}_{\ell,m} Y_{\ell,m}(\theta, \psi), \tag{13a}$$

where

$$\sum_{\ell,m} \equiv \sum_{\ell=0}^{\infty} \sum_{m=-\ell}^{\ell}, \tag{13b}$$

we define the harmonic coefficients of the the ice and sea load functions, and the Heaviside increments of the ice and sea load functions as $I_{\ell,m}$, $S_{\ell,m}$, $\delta I_{\ell,m}$ and $\delta S_{\ell,m}$, respectively. Throughout this analysis we adopt the following normalization of the spherical harmonic basis functions:

$$\iint_\Omega Y_{\ell',m'}^\dagger(\theta, \psi) Y_{\ell,m}(\theta, \psi) \sin\theta d\theta d\psi = 4\pi \delta_{\ell',\ell} \delta_{m',m}, \tag{14}$$

where † denotes the complex conjugate. The spatial convolution in (10) can now be performed analytically by applying the result (e.g. Mitrovica & Peltier 1991)

$$\iint_\Omega \mathscr{X}(\theta, \psi) P_\ell(\cos\gamma)\, d\Omega' = \frac{4\pi}{(2\ell+1)} \sum_{m=-\ell}^{\ell} \mathscr{X}_{\ell,m} Y_{\ell,m}(\theta, \psi). \tag{15}$$

This leads to the following spectral-domain form of the sea-level equation for a Maxwell viscoelastic, non-rotating earth model excited by a Heaviside loading history (Mitrovica & Peltier 1991):

$$\begin{aligned} &\sum_{\ell,m} S_{\ell,m}(t) Y_{\ell,m}(\theta, \psi) \\ &= C(\theta, \psi, t) \sum_{\ell,m} \Bigg\{ E_\ell^{\mathrm{L}} T_\ell (\rho_{\mathrm{i}} I_{\ell,m}(t) + \rho_{\mathrm{w}} S_{\ell,m}(t)) \\ &\quad + T_\ell \sum_{n=1}^{N} (\rho_{\mathrm{i}} \delta I_{\ell,m}^n + \rho_{\mathrm{w}} \delta S_{\ell,m}^n) \beta_\ell^{\mathrm{L}}(t-t_n) H(t-t_n) \\ &\quad + \frac{\Delta\Phi^{\mathrm{L}}(t)}{g} \delta_{l,0} \delta_{m,0} \Bigg\} Y_{\ell,m}(\theta, \psi), \end{aligned} \tag{16}$$

where

$$T_\ell = \frac{4\pi a^3}{M_{\mathrm{e}}(2\ell+1)}. \tag{17}$$

2.2 The sea-level equation for a rotating Earth

On a rotating Earth, the geoid and solid surface are perturbed by a changing rotational potential as well as by a changing surface load. The sea-level response of our earth model to a time-varying potential excitation can be calculated using a method which is analogous to that used in the loading problem described above. To calculate the sea-level response to a varying potential, as opposed to a surface load, we invoke the use of tidal Love numbers that describe the response of the earth model to a general potential forcing that does not involve a loading of the Earth's surface. In the following, we first derive the rotational contribution to the sea-level equation and then proceed to discuss the form of the perturbing rotational potential.

When subject to a changing rotational potential, the sea-level response of our earth model depends on the viscoelastic tidal Love numbers,

$$h_\ell^{\mathrm{T}}(t) = h_\ell^{\mathrm{T,E}} \delta(t) + \sum_{k=1}^{K} r_k^{\ell,\mathrm{T}} \exp(-s_k^\ell t) \tag{18}$$

and

$$k_\ell^{\mathrm{T}}(t) = k_\ell^{\mathrm{T,E}} \delta(t) + \sum_{k=1}^{K} r_k'^{\ell,\mathrm{T}} \exp(-s_k^\ell t), \tag{19}$$

where the superscript T indicates parameters associated with a general potential (tidal) forcing. Eqs (18) and (19) are the tidal analogues to the load Love numbers in eqs (1) and (2), and they can be used to estimate the Earth's response to a general potential forcing. [Note that the inverse decay times, s_k^ℓ, in eqs (18) and (19) are the same as those associated with the load-induced deformation in (1) and (2).] The tidal Green's functions for the gravitational potential perturbation at the undeformed surface and the radial displacement of the solid surface are, respectively,

$$\Phi_\ell^{\mathrm{T}}(t) = \delta(t) + k_\ell^{\mathrm{T,E}} \delta(t) + \sum_{k=1}^{K} r_k'^{\ell,\mathrm{T}} \exp(-s_k^\ell t) \tag{20}$$

and

$$\Gamma_\ell^{\mathrm{T}}(t) = \frac{1}{g} \left[h_\ell^{\mathrm{T,E}} \delta(t) + \sum_{k=1}^{K} r_k^{\ell,\mathrm{T}} \exp(-s_k^\ell t) \right]. \tag{21}$$

In contrast to the loading Green's functions in eqs (3) and (4), (20) and (21) are Green's functions in time only. That is, the perturbations to the geopotential and the solid surface radial displacement are calculated by convolving the time variation of the rotational potential with (20) and (21). In analogy with eq. (3), the first Dirac delta function on the right-hand side of (20) signifies the direct effect of the rotational potential on the Earth's gravity field.

Let us denote the harmonic coefficients of the perturbing rotational potential as $\Lambda_{\ell,m}(t)$; the deflections of the geoid and the radial position of the solid surface are then given by

$$G_{\ell,m}^{\mathrm{T}}(t) = \frac{1}{g} \int_{-\infty}^{t} \Lambda_{\ell,m}(t') \Phi_\ell^{\mathrm{T}}(t-t')\, dt' + \frac{\Delta\Phi^{\mathrm{T}}(t)}{g} \delta_{\ell,0} \delta_{m,0} \tag{22}$$

and

$$R_{\ell,m}^{\mathrm{T}}(t) = \int_{-\infty}^{t} \Lambda_{\ell,m}(t') \Gamma_\ell^{\mathrm{T}}(t-t')\, dt'. \tag{23}$$

To be consistent with eq. (9), we model the temporal form of the rotational potential as a series of Heaviside increments:

$$\Lambda_{\ell,m}(t) = \sum_{n=1}^{N} \delta\Lambda_{\ell,m}^n H(t-t_n). \tag{24}$$

GJI000 24/3/98 10:31:45 3B2 version 5.20
The Charlesworth Group, Huddersfield 01484 517077

Using eq. (24) in (22) and (23) and applying (13) we obtain the following expressions:

$$G^{\mathrm{T}}(\theta,\psi,t)=\sum_{\ell,m}\left\{(1+k_\ell^{\mathrm{T,E}})\,\frac{\Lambda_{\ell,m}(t)}{g}+\sum_{n=1}^{N}\frac{\delta\Lambda_{\ell,m}^{n}}{g}\sum_{k=1}^{K}\frac{r_k'^{\ell,\mathrm{T}}}{s_k^\ell}\right.$$

$$\left.\times[1-\exp(-s_k^\ell(t-t_n))]+\frac{\Delta\Phi^{\mathrm{T}}(t)}{g}\,\delta_{\ell,0}\delta_{m,0}\right\}Y_{\ell,m}(\theta,\psi) \tag{25}$$

and

$$R^{\mathrm{T}}(\theta,\psi,t)=\sum_{\ell,m}\left\{h_\ell^{\mathrm{T,E}}\,\frac{\Lambda_{\ell,m}(t)}{g}+\sum_{n=1}^{N}\frac{\delta\Lambda_{\ell,m}^{n}}{g}\sum_{k=1}^{K}\frac{r_k^{\ell,\mathrm{T}}}{s_k^\ell}\right.$$

$$\left.\times[1-\exp(-s_k^\ell(t-t_n))]\right\}Y_{\ell,m}(\theta,\psi)\,. \tag{26}$$

The difference between (25) and (26) multiplied by the ocean function gives the contribution of the varying rotational potential forcing to sea-level change. Adding this contribution to eq. (16) yields

$$\sum_{\ell,m}S_{\ell,m}(t)\,Y_{\ell,m}(\theta,\psi)$$

$$=C(\theta,\psi,t)\sum_{\ell,m}\left\{E_\ell^{\mathrm{L}}T_\ell(\rho_{\mathrm{i}}I_{\ell,m}(t)+\rho_{\mathrm{w}}S_{\ell,m}(t))+E_\ell^{\mathrm{T}}\,\frac{\Lambda_{\ell,m}(t)}{g}\right.$$

$$+\sum_{n=1}^{N}\left[T_\ell(\rho_{\mathrm{i}}\delta I_{\ell,m}^{n}+\rho_{\mathrm{w}}\delta S_{\ell,m}^{n})\beta_\ell^{\mathrm{L}}(t-t_n)+\frac{\delta\Lambda_{\ell,m}^{n}}{g}\,\beta_\ell^{\mathrm{T}}(t-t_n)\right]$$

$$\left.\times H(t-t_n)+\frac{\Delta\Phi(t)}{g}\,\delta_{\ell,0}\delta_{m,0}\right\}Y_{\ell,m}(\theta,\psi)\,, \tag{27}$$

with

$$E_\ell^{\mathrm{T}}=1+k_\ell^{\mathrm{T,E}}-h_\ell^{\mathrm{T,E}} \tag{28a}$$

and

$$\beta_\ell^{\mathrm{T}}(t-t_n)=\sum_{k=1}^{K}\frac{(r_k'^{\ell,\mathrm{T}}-r_k^{\ell,\mathrm{T}})}{s_k^\ell}\,[1-\exp(-s_k^\ell(t-t_n))]\,. \tag{28b}$$

Eq. (27) is the spectral domain form of the sea-level equation for a Maxwell viscoelastic earth model excited by both a surface mass load redistribution and a changing rotational potential (both varying with a Heaviside time dependence). We now consider the form of the rotational potential and how it can be calculated.

2.3 The rotational potential

In the following analysis we use a right-handed Cartesian coordinate system denoted by (x_i) with its origin located at the centre of mass of the earth model in its unperturbed state. The x_1 axis is aligned along Greenwich longitude and the x_2 axis is 90° east of x_1. In the equilibrium state (that is before surface loading), the rotation vector, $\boldsymbol{\omega}(t)$, is assumed to be $(0, 0, \Omega)$. Subsequent to the onset of surface mass redistribution, the inertia tensor of the system is perturbed and the components $\omega_i (i=1, 2)$ generally become non-zero. It is conventional to write the ω_i in the form

$$\omega_i(t)=\Omega(\delta_{i3}+m_i(t)) \tag{29}$$

(e.g. Munk & MacDonald 1960), where the $m_i(t)$ are small changes from the equilibrium state.

The rotational potential at the surface of a spherical earth can be written in the form

$$U_R(\gamma)=\frac{1}{3}\,\omega^2a^2-\frac{1}{3}\,\omega^2a^2P_{2,0}(\cos\gamma) \tag{30}$$

(e.g. Lambeck 1980), where γ is now the angular distance between $\boldsymbol{\omega}(t)$ and an arbitrary field point (θ, ψ). Using the result

$$P_{2,0}(\cos\gamma)=\frac{1}{5}\sum_{m=-2}^{2}Y_{2,m}^{\dagger}(\theta',\psi')\,Y_{2,m}(\theta,\psi) \tag{31}$$

in eq. (30), where (θ', ψ') are the coordinates of $\boldsymbol{\omega}(t)$, we obtain the following expression for the perturbation to the rotational potential from the equilibrium value:

$$\Lambda(\theta,\psi,t)=\Lambda_{0,0}(t)\,Y_{0,0}(\theta,\psi)+\sum_{m=-2}^{2}\Lambda_{2,m}(t)\,Y_{2,m}(\theta,\psi)\,, \tag{32}$$

where

$$\Lambda_{0,0}(t)=\frac{a^2\Omega^2}{3}\,[m^2(t)+2m_3(t)]\,, \tag{33a}$$

$$\Lambda_{2,0}(t)=\frac{a^2\Omega^2}{6\sqrt{5}}\,[m_1^2(t)+m_2^2(t)-2m_3^2(t)-4m_3(t)]\,, \tag{33b}$$

$$\Lambda_{2,1}(t)=\frac{a^2\Omega^2}{\sqrt{30}}\,[m_1(t)(1+m_3(t))-\mathrm{i}m_2(t)(1+m_3(t))]\,, \tag{33c}$$

$$\Lambda_{2,2}(t)=\frac{a^2\Omega^2}{\sqrt{5}\sqrt{24}}\,[(m_2^2(t)-m_1^2(t))+\mathrm{i}2m_1(t)m_2(t)]\,, \tag{33d}$$

with

$$\Lambda_{2,-m}=(-1)^m\Lambda_{2,m}^{\dagger}\,. \tag{33e}$$

The symbol i in eq. (33) represents the complex number $\sqrt{-1}$. Note that the rotational potential is completely described by degree 0 and degree 2 harmonics. Our calculations show that the m_3 perturbations due to GIA are several orders of magnitude smaller than either m_1 or m_2. As a consequence, the $\Lambda_{2,1}(t)$ term in eq. (33) is dominant since it is the only coefficient of the perturbed potential which contains first-order terms in m_1 or m_2 (neglecting the other harmonic components would introduce an error of no more than ~1 per cent). Therefore, the sea-level response due to GIA will be dominated by the degree 2 order 1 harmonic signature (as discussed by Han & Wahr 1989).

A number of publications describe the theory used to determine the m_i associated with the surface loading of a spherically symmetric, Maxwell viscoelastic earth model. The two most commonly adopted methodologies are described, e.g. in Sabadini *et al.* (1982) and Wu & Peltier (1984). Although these two approaches are similar, the final equations used to calculate the m_i are different. Recent work by Vermeersen & Sabadini (1996) and Mitrovica & Milne (1997) has shown, however, that these two methodologies yield essentially the same GIA-induced m_i for a specific load and earth model. In this study, we apply the equations derived by Wu & Peltier

GJI000 24/3/98 10:32:08 3B2 version 5.20
The Charlesworth Group, Huddersfield 01484 517077

(1984). These are

$$\langle m_i(t)\rangle = \frac{\Omega}{A\sigma_0}\left[D_1 J_{i3}^{\mathrm{L}}(t) + D_2\int_0^t J_{i3}^{\mathrm{L}}(t')dt' + \sum_{k=1}^{K-1} E_k(J_{i3}^{\mathrm{L}}(t) * \exp(-\lambda_k t))\right] \quad (i=1,\,2)\,, \tag{34a}$$

and

$$m_3(t) = -\frac{1}{C}\left[D_1 J_{33}^{\mathrm{L}}(t) + \sum_{k=1}^{K} r_k^{\ell=2,L}(J_{33}^{L}(t) * \exp(-s_k^{\ell=2}t))\right], \tag{34b}$$

where the $*$ denotes temporal convolution. C is the polar moment of inertia in the unperturbed state. We assume the two equatorial moments of inertia in this state are equal and we denote them by A. The symbol $\langle\ \rangle$ signifies that the Chandler wobble has been removed from the response. Furthermore, the λ_k are roots of the polynomial

$$Q(s) = \frac{\sum_{q=1}^{K}\left[\dfrac{r_q'^{\ell=2,\mathrm{T}}}{s_q^{\ell=2}}\prod_{p\neq q}(s+s_p^{\ell=2})\right]}{\sum_{j=1}^{K}\dfrac{r_j'^{\ell=2,\mathrm{T}}}{s_j^{\ell=2}}}\,. \tag{35}$$

Also,

$$D_1 = 1 + k_2^{\mathrm{L,E}}\,, \tag{36}$$

$$D_2 = \frac{l_s\prod_{p=1}^{K} s_p^{\ell=2}}{\prod_{p=1}^{K-1}\lambda_p} \tag{37}$$

and

$$E_k = -\frac{\left[\dfrac{l_s\prod_{p=1}^{K}(s_p^{\ell=2}-\lambda_k)}{\lambda_k} + \sum_{q=1}^{K}\dfrac{r_q'^{\ell=2,L}}{s_q^{\ell=2}}\prod_{p\neq q}(s_p^{\ell=2}-\lambda_k)\right]}{\prod_{q\neq k}^{K-1}(\lambda_q-\lambda_k)}\,. \tag{38}$$

The parameter σ_o in (34a) is the Chandler wobble frequency of a deformable Maxwell viscoelastic earth model and is given by

$$\sigma_0 = \frac{\sigma_{\mathrm{r}}}{k_{\mathrm{f}}}\sum_{p=1}^{K}\frac{r_p'^{\ell=2,\mathrm{T}}}{s_p^{\ell=2}}\,, \tag{39}$$

where σ_{r} is the Euler wobble frequency, given by

$$\sigma_{\mathrm{r}} = \Omega\left(\frac{C}{A}-1\right), \tag{40}$$

and k_{f} is the fluid k Love number, defined as

$$k_{\mathrm{f}} = k_2^{\mathrm{T,E}} + \sum_{p=1}^{K}\frac{r_p'^{\ell=2,\mathrm{T}}}{s_p^{\ell=2}}\,. \tag{41}$$

Finally,

$$l_s = 1 + k_2^{\mathrm{L,E}} + \sum_{p=1}^{K}\frac{r_p'^{\ell=2,\mathrm{L}}}{s_p^{\ell=2}}\,. \tag{42}$$

The $J_{i3}^{\mathrm{L}}(t)$ in eq. (34) are the perturbations to the $i3$th component of the inertia tensor due to the direct effect of the redistribution of the surface load. Wu & Peltier (1984) derived expressions for the $J_{i3}^{\mathrm{L}}(t)$ for the case of highly simplified disc load geometries. We have derived general expressions which relate the $J_{i3}^{\mathrm{L}}(t)$ to the spherical harmonic coefficients of an arbitrary surface load. These expressions are

$$[\delta J_{13}^{L}]^n = \frac{4}{3}\sqrt{\frac{6}{5}}\,a^4\pi\,\mathscr{R}e[\rho_{\mathrm{i}}\delta I_{21}^n + \rho_{\mathrm{w}}\delta S_{21}^n]\,, \tag{43a}$$

$$[\delta J_{23}^{L}]^n = -\frac{4}{3}\sqrt{\frac{6}{5}}\,a^4\pi\,\mathscr{I}m[\rho_{\mathrm{i}}\delta I_{21}^n + \rho_{\mathrm{w}}\delta S_{21}^n]\,, \tag{43b}$$

$$[\delta J_{33}^{L}]^n = \frac{8}{3}\,a^4\pi\left[\mathscr{R}e(\rho_{\mathrm{i}}\delta I_{00}^n + \rho_{\mathrm{w}}\delta S_{00}^n) - \frac{1}{\sqrt{5}}\,\mathscr{R}e(\rho_{\mathrm{i}}\delta I_{20}^n + \rho_{\mathrm{w}}\delta S_{20}^n)\right] = -\frac{8\pi}{3\sqrt{5}}\,a^4\,\mathscr{R}e(\rho_{\mathrm{i}}\delta I_{20}^n + \rho_{\mathrm{w}}\delta S_{20}^n)\,, \tag{43c}$$

with

$$J_{i3}^{\mathrm{L}}(t) = \sum_{n=1}^{N}[\delta J_{i3}^n]H(t-t_n)\,. \tag{44}$$

Note that from eqs (34) and (43) the m_i are dependent on the sea-level load $S(\theta, \psi, t)$; therefore, sea-level change appears explicitly on the right-hand side of (27) as a contributor to the surface mass load and implicitly as a functional argument of the perturbation to the rotational potential.

2.4 Solving the sea-level equation

To solve the sea-level equation (27) in a gravitationally self-consistent manner with a time-dependent ocean function, we have modified the pseudo-spectral method described in Mitrovica & Peltier (1991). By defining the load and rotational potential as a series of Heaviside increments in time, solving (27) reduces to determining the $\delta S_{\ell,m}^n$ for successive values of n ($n=1,\,2,\,3,\,\ldots$). Let us consider the jth Heaviside increment. This increment, which represents a combination of an ice–ocean load and a perturbing rotational potential, is applied at t_j and we can write

$$\delta S_{\ell,m}^j = S_{\ell,m}(t_j) - S_{\ell,m}(t_{j-1})\,. \tag{45}$$

At any time $t=t_j$ it is assumed that sea level at the previous time step, $t=t_{j-1}$, has been computed. Using eq. (45) in (27) we have, for $t=t_j$,

$$\sum_{\ell,m}[S_{\ell,m}(t_{j-1}) + \delta S_{\ell,m}^j]Y_{\ell,m}(\theta,\psi) = C(\theta,\psi,t)\sum_{\ell,m}\left\{E_\ell^{\mathrm{L}}T_\ell(\rho_{\mathrm{i}}I_{\ell,m}(t) + \rho_{\mathrm{w}}S_{\ell,m}(t_{j-1})) + E_\ell^{\mathrm{T}}\frac{\Lambda_{\ell,m}(t_{j-1})}{g} + \left[E_\ell^{\mathrm{L}}T_\ell\delta S_{\ell,m}^j + E_\ell^{\mathrm{T}}\frac{\delta\Lambda_{\ell,m}^j}{g}\right] + \sum_{n=1}^{j-1}\left[T_\ell(\rho_{\mathrm{i}}\delta I_{\ell,m}^n + \rho_{\mathrm{w}}\delta S_{\ell,m}^n)\beta_\ell^{\mathrm{L}}(t_j-t_n) + \frac{\delta\Lambda_{\ell,m}^n}{g}\,\beta_\ell^{\mathrm{T}}(t_j-t_n)\right] + \frac{\Delta\Phi(t_j)}{g}\,\delta_{\ell,0}\delta_{m,0}\right\}Y_{\ell,m}(\theta,\psi)\,. \tag{46}$$

GJI000 24/3/98 10:32:40 3B2 version 5.20
The Charlesworth Group, Huddersfield 01484 517077

The solution of (46) requires two nested numerical iterations. In the first iteration we plug a first guess for $\delta S^j_{\ell,m}$ into the right-hand side of eq. (46). In practice, this first guess is the eustatic change in sea level defined by

$$[\delta S^j_{\ell,m}]^{i=1} = \left[-\frac{\rho_i}{\rho_w} \frac{\delta I^j_{00}}{C_{00}(t_j)} \right] C_{\ell m}(t_j) \tag{47}$$

(e.g. Mitrovica & Peltier 1991), where the superscript $i=1$ denotes the first iterate of $\delta S^j_{\ell,m}$, and the $C_{\ell m}(t_j)$ are the spherical harmonic coefficients of the ocean function $C(\theta, \psi, t_j)$. This is then used to calculate $[\delta \Lambda^j_{\ell,m}]^{i=1}$ via eqs (33)–(44). The second iterate of sea-level change, $[\delta S^j_{\ell,m}]^{i=2}$, is then determined by solving the right-hand side of eq. (46) using these approximations. This procedure is repeated until

$$\sum_{\ell,m} \frac{|[\delta S^j_{\ell,m}]^{i+1}| - |[\delta S^j_{\ell,m}]^i|}{|[\delta S^j_{\ell,m}]^i|} < \epsilon, \tag{48}$$

where ϵ is a pre-determined convergence parameter and the vertical bars represent the modulus of the complex variable. We have found, using $\epsilon = 10^{-4}$, that three to five iterations are required for convergence.

The second iteration in the solution involves the inclusion of a time-dependent ocean function $C(\theta, \psi, t)$. During periods of glacial accumulation or ablation, the ocean periphery changes form, largely due to ice margin migration and sea-level change. To date, most sea-level calculations have adopted a fixed ocean function which is assumed to be identical to the present-day ocean–land geometry (e.g. Mitrovica & Peltier 1991). Clearly, in near-field areas the ocean boundary has changed significantly due to the wax and wane of the ice sheets (e.g. Tushingham & Peltier 1991). However, the ocean–land boundary has also changed significantly where the continental shelf is relatively shallow (e.g. Johnston 1993). Incorporating a time-dependent ocean function into the sea-level algorithm described above is non-trivial since the ocean–land interface is required to define completely the ocean load geometry, so any change in $C(\theta, \psi, t)$ will affect the predicted sea level. Therefore, to obtain accurate solutions of $C(\theta, \psi, t)$, and thus sea level, a second iterative process is required. In this regard, we first define a series of ocean functions $C(\theta, \psi, t_j)$, where $j=1, n$, and each t_j corresponds to the timing of the Heaviside events described above. In practice, as a first guess, we assume that the $C(\theta, \psi, t_j)$ are only dependent on the migration of the ice–ocean boundary defined by the adopted ice model. That is, we assume a present-day coastline geometry except in 'near-field' regions where the ice migrates into present-day ocean areas. Using this first series of ocean functions we solve the sea-level equation and predict global relative sea level at each $t=t_j$. Then, by subtracting the relative (to present day) sea-level signal at each t_j from a present-day global topography data set, we calculate a second iterate set of $C(\theta, \psi, t_j), j=1, n$. This procedure, which is adopted from earlier analyses (e.g. Johnston 1993; Peltier 1994), is repeated until a desired convergence is attained (one or two iterations are normally adequate). The results shown in the next section were calculated using the third iterate set of ocean functions.

As mentioned in the Introduction, perturbations to the Earth's rotation vector are caused by a number of processes acting over different timescales. For example, recent calculations have shown that convective flow within the mantle may contribute significantly to the present-day secular motion of the rotation pole (Steinberger & O'Connell 1997). It is of interest, therefore, to consider how the theory described above can be modified to calculate sea-level change resulting from an *a priori* defined polar wander path. For this case, the governing equation is a modified form of eq. (27) in which the $\delta I^n_{\ell,m}$ and $I_{\ell,m}(t)$ are set to zero. This equation can be solved using the same iterative approach discussed above. The only difference is that the first iterate of the sea-level increment, $[\delta S^n_{l,m}]^{i=1}$, is set to zero [this follows from setting $\delta I_{00}=0$ in eq. (47)].

As a final point, we will frequently discuss RSL variations in the following sections. We define these as $RSL(\theta, \psi, t) = S(\theta, \psi, t_j) - S(\theta, \psi, t_p)$, where t_p is the present day.

3 RESULTS

Calculations were carried out using a spherically symmetric, self-gravitating, compressible, Maxwell viscoelastic earth model which has an elastic structure defined by PREM (Dziewonski & Anderson 1981). The upper-mantle viscosity (ν_{um}) is fixed at 10^{21} Pa s and the lower-mantle viscosity (ν_{lm}) and the lithospheric thickness (LT) are variable parameters in the modelling. The ice model used is based on the global ICE-3G deglaciation history proposed by Tushingham & Peltier (1991). We construct a $\sim$100 kyr glaciation phase by reversing the ICE-3G deglaciation history and extending it appropriately in time. The ice load is temporally discretized into a series of Heaviside loading increments spaced at 7 kyr intervals during glaciation and 1 kyr intervals during deglaciation. Spherical harmonic representations are expanded to degree and order 128.

Since polar wander is sensitive to the number of glacial cycles included in the modelling calculation (e.g. Wu & Peltier 1984), it is necessary to determine whether postglacial RSL predictions are also sensitive to this parameter. Fig. 1 shows the predicted rotational contribution to RSL at Clinton, MA (northeastern United States), after one glacial cycle and seven glacial cycles for an isoviscous mantle of 10^{21} Pa s and a lithospheric thickness of 120 km. We have found that this particular viscosity structure yields the maximum difference between the one and seven cycle predictions for the suite of earth models we have considered. Nevertheless, the discrepancy is (in general) less than a tenth of a metre. Accordingly, we adopt one glacial cycle in the subsequent analysis.

An example of the spatial form of the sea-level signal associated with GIA perturbations to the rotation vector is shown in Fig. 2. (Note, the reader can compare this rotation-induced RSL signal to the 'non-rotating' case by referring to Fig. 4, which shows RSL curves at a number of globally distributed sites calculated by solving the new and the conventional sea-level equation.) This figure is obtained by differencing a prediction calculated using the new sea-level theory (eq. 27) with one based on the theory appropriate to a non-rotating Earth (eq. 17). For comparison, Fig. 3 shows the analogous sea-level change associated with the direct effect of the perturbing rotational potential alone (that is the sea load induced by the rotational forcing is not considered). Figs 2 and 3 were computed using the same earth model and both represent global plots of RSL at 18 kyr BP. As discussed

GJI000 24/3/98 10:33:11 3B2 version 5.20
The Charlesworth Group, Huddersfield 01484 517077

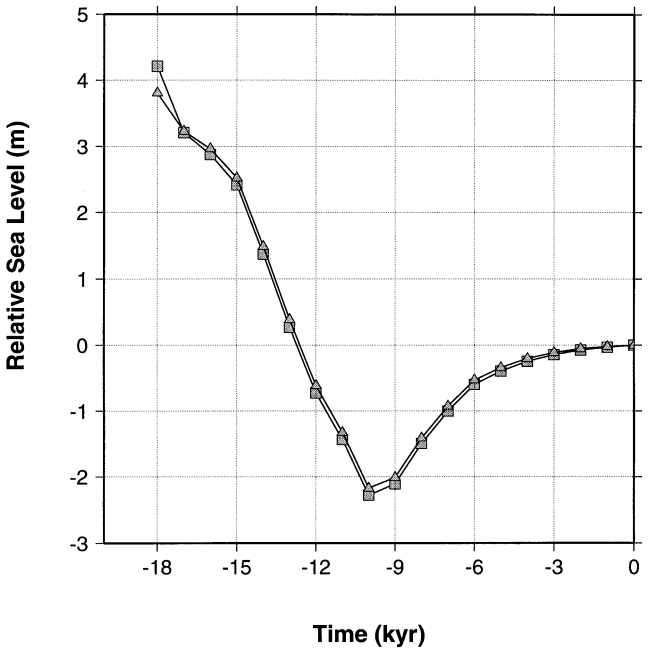

Figure 1. The postglacial RSL signal at Clinton (41.2N, −72.5E) caused by GIA-induced variations in the Earth's rotation vector calculated using an earth model with an isoviscous mantle of 10^{21} Pa s and a lithospheric thickness (LT) of 120 km. The squares indicate predictions calculated using a single glacial cycle, while the triangles show predictions calculated using seven glacial cycles.

in the context of eq. (33), Figs 2 and 3 are dominated by a degree 2 order 1 harmonic signal (the combined contribution of orders 0 and 2 is less than ∼1 per cent). A comparision of Figs 2 and 3 indicates that the ocean load deformation associated with the rotational signal excites higher-degree harmonics (note the short-wavelength structure in Fig. 2) and acts, in general, to increase the amplitude of the RSL signal. For example, the total RSL signal range in Fig. 3 is ∼9 m, which compares with ∼12 m in Fig. 2. This increase in amplitude can be explained in a straightforward manner. Consider, for example, the east coast of North America. The direct effect of the rotational potential induces a sea-level fall of approximately 4–5 m over the last 18 kyr in this region (see Fig. 3). This sea-level fall represents a 'negative' load which will be accompanied, in the full calculation, by an incremental uplift of the solid Earth. This uplift acts to increase the amplitude of the predicted sea-level fall and hence the results in Fig. 2 show an enhanced sea-level fall in this region of about 5–6 m. This enhancement is evident in both the western Atlantic and the southern Indian Ocean. A related effect occurs over southern South America and Japan. In this case the sea-level rise associated with the direct effect of the perturbing rotational potential (from 18 kyr BP to present) acts to induce an incremental solid surface subsidence and hence an enhanced sea-level rise. Clearly, an accurate prediction of rotation-induced postglacial sea level requires the application of the gravitationally self-consistent theory of eq. (27).

Since the dominant degree 2 order 1 sea-level signal is due to polar wander, as opposed to change in the length of day, the spatial orientation of the signal is, to a large extent, defined by the line of longitude along which the rotation pole moves, on average, during deglaciation (Han & Wahr 1989; MM). Our predictions show that the rotation pole traces an average direction along the great circle defined by longitudes ∼106°E, ∼74°W, with the pole moving towards Hudson Bay during the deglaciation phase. Therefore, the rotational potential will show maximum change along this meridian at mid-latitudes and a minimum change at both 90 longitudinal degrees from this meridian and along the equator. The sea-level signals shown in Figs 2 and 3 clearly reflect this pattern.

The temporal form of the rotation-induced sea-level signal is evident in Fig. 4, which shows predicted RSL curves for rotating and non-rotating Earth models (left side) and the difference between these (rotating minus non-rotating; right side) for sites distributed around the globe. As in Figs 2 and 3, these predictions were calculated using an earth model with $LT = 120$ km, $\nu_{\rm um} = 10^{21}$ Pa s and $\nu_{\rm lm} = 10^{22}$ Pa s. The specific sites were chosen to illustrate the spatial symmetry and maximum and minimum amplitudes of the rotation-induced sea-level signal. [Clinton and Recife were also chosen to facilitate comparison with the results of Han & Wahr (1989)—see below.] Most of the sites included in Fig. 4 are from far-field regions where the predicted RSL curves are not significantly affected by ice-induced deformation (Tientsin, Perth, Recife and Bremerhaven fall into this category). The site 'Bahia Gente Grande' is located near the southern section of the Andes mountain range, where a small ice mass existed at LGM producing a significant amount of deformation. Clinton is located near the edge of the massive Laurentide ice mass and so exhibits an RSL curve that is characteristic of such regions, that is, the initial sea-level fall due to solid surface rebound is followed by sea-level rise as the peripheral bulge migrates towards the centre of the ice mass (e.g. Clark *et al.* 1978).

The symmetry of the rotation-induced sea-level signal is evident when comparing the 'rotating minus non-rotating' predictions for Clinton, Bahia Gente Grande, Tientsin and Perth. All of these sites are at mid-latitudes near the great-circle meridian described above. Sites that are 180 latitudinal degrees apart on this meridian exhibit the same time-dependent rotation-induced RSL curve (e.g. Clinton and Perth, Bahia Gente Grande and Tientsin). Sites near the equator, such as Recife, display a considerably smaller amplitude, as do sites that are located ∼90 longitudinal degrees from the polar wander meridian (e.g. Bremerhaven).

The postglacial rotation-induced sea-level signal is related to the rate of polar wander during the deglaciation period. To illustrate this relationship, consider Fig. 5, which shows polar wander (that is rotation pole displacement) (Fig. 5a), and the direct, elastic, viscous and total sea-level response to the changing rotational potential at the site Clinton (Fig. 5b). Note, first, that the direct and elastic effects are proportional to the time-series of polar wander, whereas the viscous effect is a time-lagged response to the displacement of the rotation pole. The direct effect of the rotational potential acts to produce a sea-level fall at this site during deglaciation, whereas the viscoelastic deformation associated with the rotational potential is dominated by solid surface subsidence and sea-level rise. Notice that the direct effect dominates the rotation-induced sea-level signal until about half way through the deglaciation phase (∼9–12 kyr BP). Subsequent to this time, the viscoelatic deformation, particularly the non-elastic component of this deformation, dominates. This evolution in the strength of the direct and

GJI000 24/3/98 10:33:33 3B2 version 5.20
The Charlesworth Group, Huddersfield 01484 517077

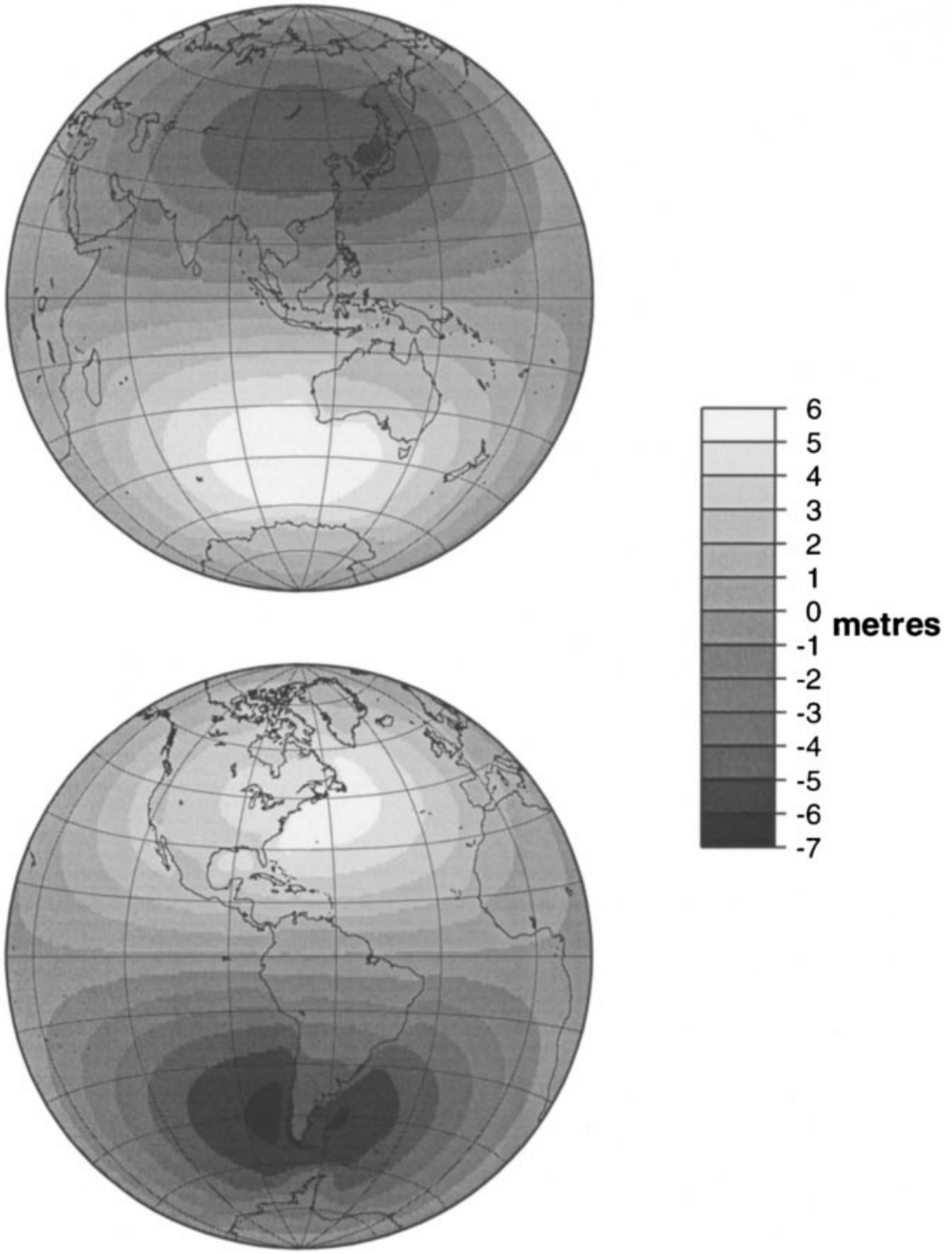

Figure 2. The predicted global signal of RSL at 18 kyr BP (that is the change in sea level from 18 kyr BP to the present) produced by GIA-induced perturbations to the Earth's rotation vector. The earth model adopted in the calculation is characterized by $LT = 120$ km, $\nu_{um} = 10^{21}$ Pa s and $\nu_{lm} = 10^{22}$ Pa s. Note the dominant degree 2 order 1 spherical harmonic component of the signal. The shorter-wavelength harmonics are caused by the effect of the water load induced by the perturbation to the rotation vector.

viscous contributions leads to the marked non-monotonicity of the rotation-induced sea-level signals shown in all frames of Fig. 4.

Previous studies have shown that predictions of polar wander are sensitive to variations in ν_{lm} and lithospheric thickness (e.g. Yuen, Sabadini & Boschi 1982; Wu & Peltier 1984) and are relatively insensitive to variations in ν_{um} (Mitrovica & Milne 1998). Accordingly, we have calculated the rotational component of sea-level change at Clinton for a suite of earth models in which ν_{lm} (Fig. 6a) and LT (Fig. 7) are varied significantly. A comparison of Figs 6(a) and 7 indicates that the RSL signal induced by perturbations in the rotation vector is more sensitive to variations in ν_{lm} than variations in LT.

GJI000 24/3/98 10:33:45 3B2 version 5.20
The Charlesworth Group, Huddersfield 01484 517077

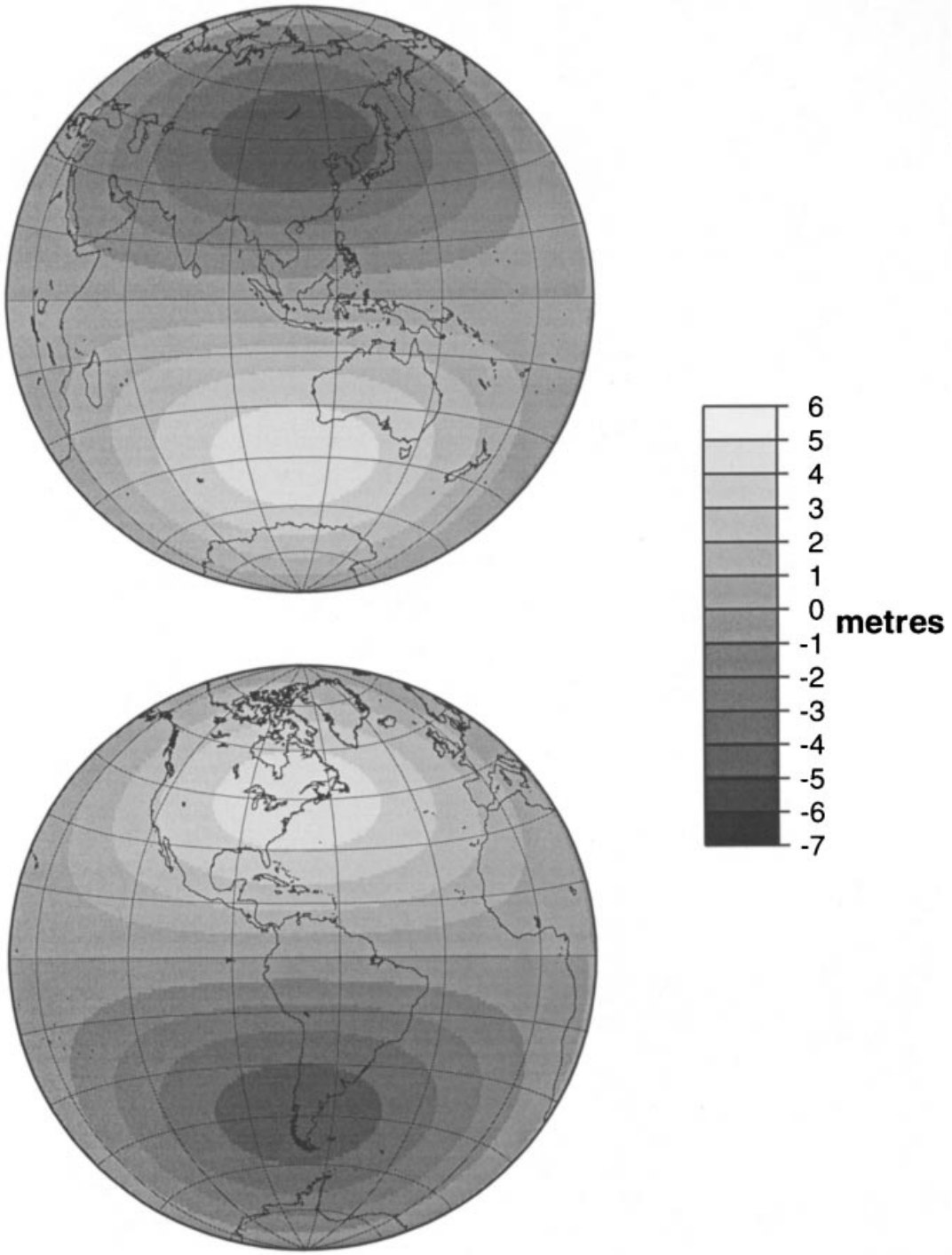

Figure 3. The predicted global signal of RSL at 18 kyr BP due to the perturbation to the rotational potential only (that is, the water loading effect associated with this potential is not considered). This prediction is based on the earth model described in Fig. 2.

Fig. 6 shows the total RSL signal associated with perturbations in the rotational potential together with the three contributions (viscous, elastic, direct) to this signal. The RSL signal at 18 kyr BP increases by a factor of ~ 2 as the lower-mantle viscosity is increased from 10^{21} to 10^{22} Pa s. This trend arises because the sea-level signal associated with viscoelastic deformation (b and c) less effectively compensates for the direct RSL contribution from the rotational potential (d) as ν_{lm} is increased.

Each prediction in Fig. 6(a) is characterized by a transition from a period of sea-level fall (prior to about 9 kyr BP) to an interval (extending to the present) of sea-level rise. Although the amplitude of the latter signal is a function of the viscoelastic structure of the adopted earth model, the timing of the transition is relatively insensitive to this structure. Once again, this timing marks the transition to a period in which the viscous response to the rotational potential dominates the direct effect of this potential.

GJI000 24/3/98 10:33:48 3B2 version 5.20
The Charlesworth Group, Huddersfield 01484 517077

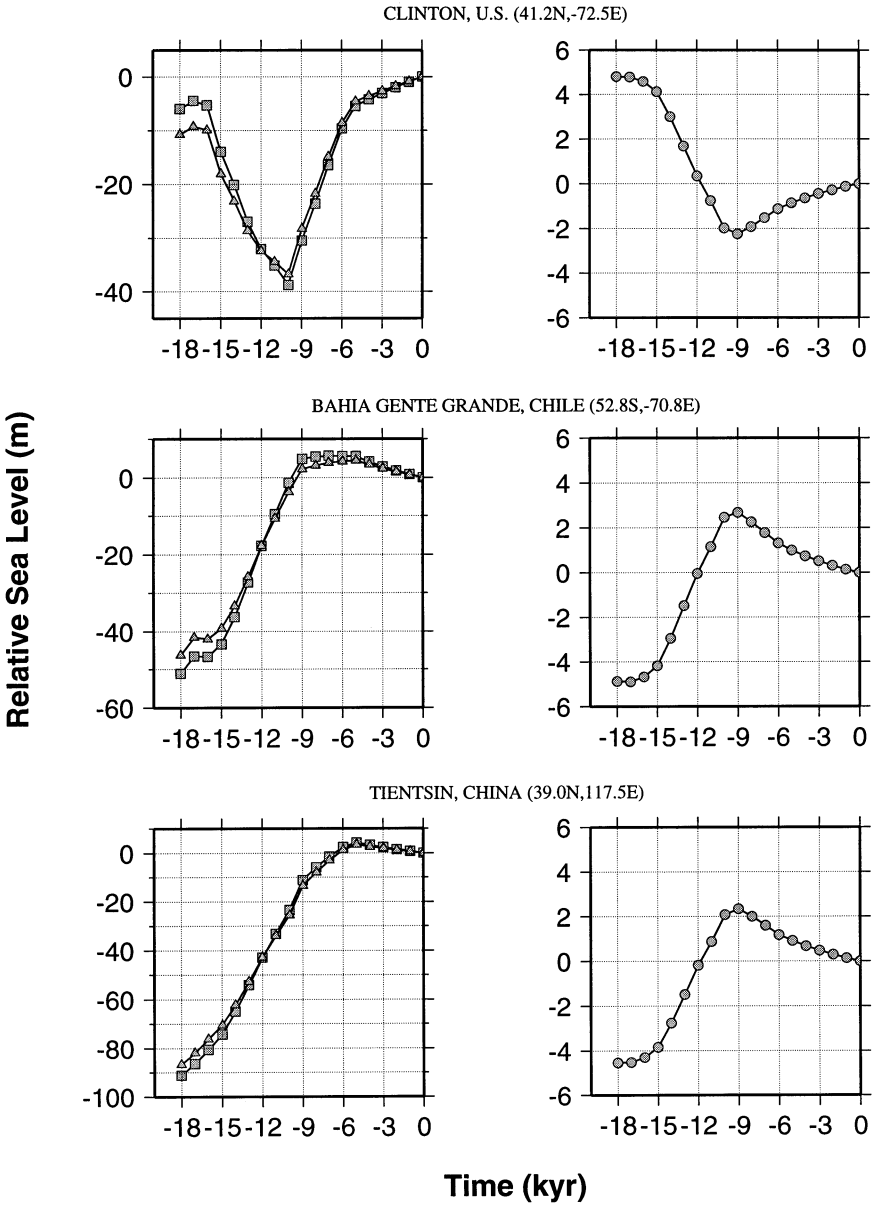

Figure 4. Postglacial RSL curves calculated using an earth model with $LT = 120$ km, $\nu_{um} = 10^{21}$ Pa s and $\nu_{lm} = 10^{22}$ Pa s. The left-hand frames show solutions of the sea-level equation for a rotating (squares) and a non-rotating (triangles) Earth. The right-hand frame shows the difference (squares minus triangles) between these predictions.

We return below to a discussion of the timing of this transition.

Fig. 7 shows the predicted rotation-induced RSL variation at Clinton for LT values of 70, 120 and 170 km with adopted ν_{lm} values of 10^{21}, 10^{22}, and 10^{23} Pa s. The results show that the rotation-induced component of RSL is most sensitive to this range of LT for the isoviscous mantle model (Fig. 7a), in which an increase in LT of 100 km leads to an increase in the predicted RSL at 18 kyr BP of $\sim$1.2 m. A similar trend is evident for models with a more viscous lower mantle (Figs 7b and c), although the sensitivity of predictions to the range of LT explored here becomes smaller as ν_{lm} is increased.

Fig. 8 shows calculated present-day rates of sea-level-change due to GIA-induced perturbations in the rotation vector. As before (see Figs 2 and 3), the signal is predominantly that of a degree 2 order 1 harmonic with some minor perturbations caused by the rotation-induced component of the water load. As in the case of RSL predictions, the rotation-induced water load also acts to increase the magnitude of the predicted signal. As an example, the rotation-induced sea load has a maximum effect in the region of southern South America, where it increases the signal magnitude by $\sim$25 per cent. This compares to an approximately 10 per cent predicted increase along the northeast coast of the US, resulting in a total peak-to-peak increase of the sea-level rate signal in the western hemisphere of $\sim$35 per cent. The prediction shown in Fig. 8 exhibits a maximum amplitude of $\sim$0.15 mm yr^{-1}. This signal amplitude is approximately 10 per cent of that recently estimated for present-day eustatic sea-level change (e.g. Peltier & Tushingham 1991; Davis & Mitrovica 1996).

GJI000 24/3/98 10:33:52 3B2 version 5.20
The Charlesworth Group, Huddersfield 01484 517077

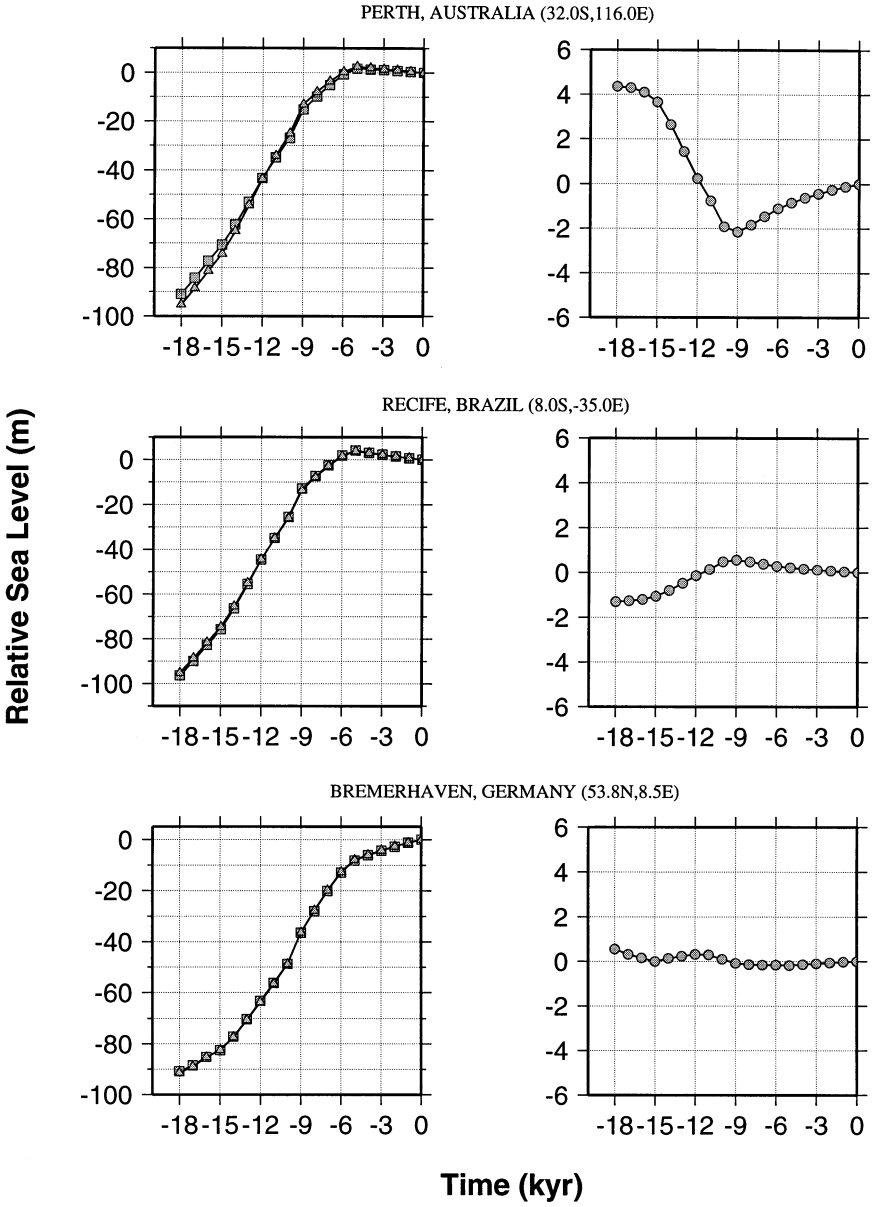

Figure 4. (*Continued.*)

We next investigate the sensitivity of the predicted, rotation-induced, rate of sea-level change to variations in lower-mantle viscosity. To illustrate this sensitivity we plot, in Fig. 9, the sea-level-change rate shown in Fig. 8 at Clinton as a function of ν_{lm} (see also Fig. 2 of MM). The predictions are remarkably insensitive to variations of ν_{lm} in the range 3×10^{21} to 50×10^{21} Pa s. The small amplitude of the prediction for $\nu_{lm} \sim 10^{21}$ Pa s may be surprising given that the predicted present-day polar wander rate for this model is large (e.g. MM). However, this small amplitude arises because the direct RSL effect due to the rotational potential is almost the same magnitude as, but of opposite sign to, the RSL signal associated with viscoelastic deformation. [This near cancellation is evident from examining the slopes of the curves in Fig. 6 (squares) at the present day.] In contrast, the predicted amplitude in the case $\nu_{lm} = 10^{23}$ Pa s is large, despite the small present-day polar wander rate prediction for this class of model (e.g. MM). In this case, the direct component of the present-day RSL response is negligible compared to the viscous component (see Fig. 6, circles). The predicted present-day rate of sea-level change based on models with ν_{lm} between these two endmembers can, analogously, be explained in the context of competing direct and viscoelastic RSL signals. Note that the predictions shown in Fig. 9 are sensitive to the amount of time elapsed since the end of the final melting event (this occurs at 5 kyr BP in the ICE 3G model). For example, if we assume the final melting event occurred 1 kyr later (at 4 kyr BP), the predicted rates would be larger, with a peak value of ~ 0.14 mm yr^{-1} associated with a ν_{lm} of 1×10^{22} Pa s. The general trend of the curve shown in Fig. 9 is not significantly altered by this modification to the ice model.

We have also considered predictions of present-day rates of sea-level change for lithospheric thicknesses ranging from 70 to 170 km while adopting the values of lower-mantle viscosity

GJI000 24/3/98 10:33:56 3B2 version 5.20
The Charlesworth Group, Huddersfield 01484 517077

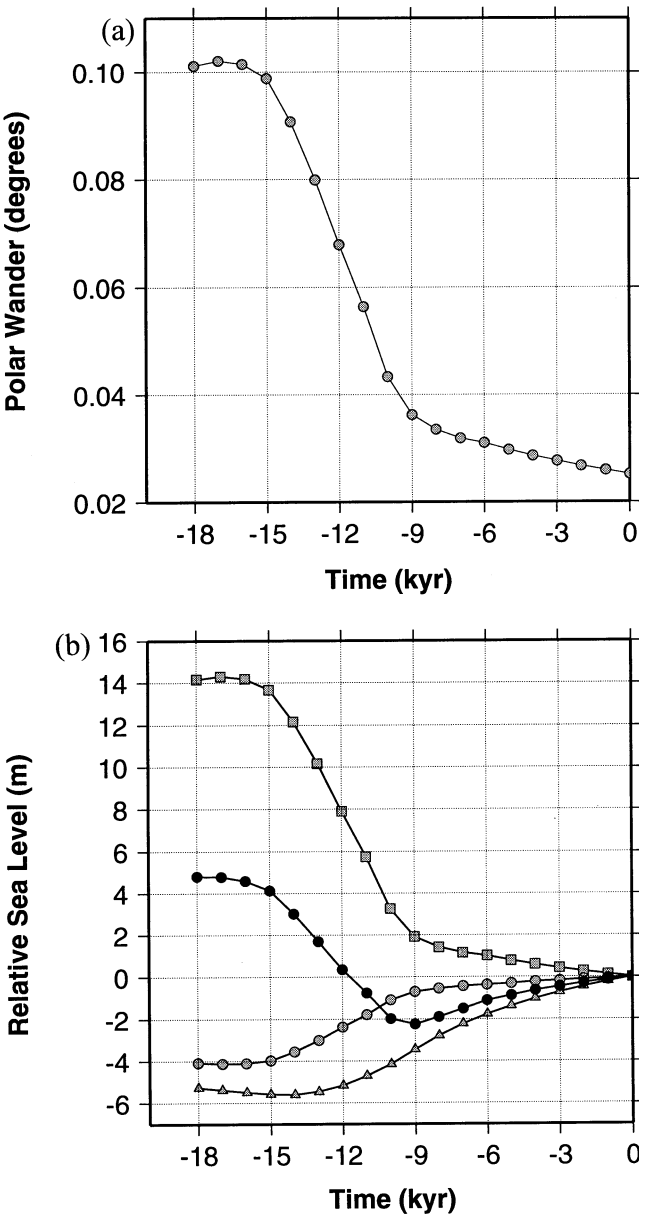

Figure 5. (a) shows the predicted GIA-induced polar wander for an earth model with $LT = 120$ km, $\nu_{um} = 10^{21}$ Pa s and $\nu_{lm} = 10^{22}$ Pa s. (b) shows the corresponding rotation-induced component of RSL at Clinton, US (41.2N, −72.5E). The squares show the direct effect of the rotational potential on sea level, while the circles and triangles show, respectively, the contributions from elastic and viscous deformations to the sea-level response. The black circles indicate the sum of these three sea-level contributions.

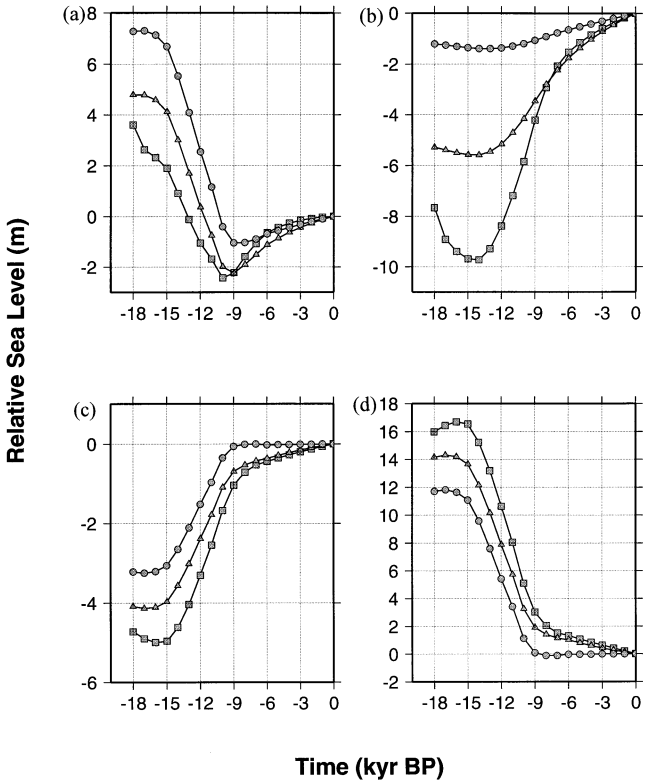

Figure 6. (a) shows the rotation-induced component of RSL at Clinton for three different earth models, each with $LT = 120$ km and $\nu_{um} = 10^{21}$ Pa s and contrasting ν_{lm} values of 10^{21} Pa s (squares), 10^{22} Pa s (triangles) and 10^{23} Pa s (circles). (b), (c) and (d) show, respectively, the viscous, elastic and direct sea-level responses contributing to the RSL signals shown in (a).

10^{21}, 10^{22} and 10^{23} Pa s. The predictions based on earth models characterized by an isoviscous mantle were most sensitive to the chosen range of LT. In this case, adopting a thin (70 km) lithosphere increased predicted rates by ∼40 per cent at selected sites, compared to the model with $LT = 120$ km, while the model with a 170 km lithosphere decreased the predicted present-day rates of sea-level change by ∼15 per cent. The sensitivity of our predictions to variations in LT for earth models with a ν_{lm} of 10^{22} or 10^{23} Pa s is approximately half of that for the isoviscous mantle models, with the same trend evident (thinner lithosphere, larger sea-level-change rate). These results, together with the predictions shown in Fig. 9, indicate that models characterized by a thin lithosphere and a factor of 5–20 increase in viscosity from upper to lower mantle will produce the largest signal. Our calculations show that such models produce maximum present-day peak-to-peak rates of ∼0.3 mm yr^{-1}.

4 DISCUSSION

In their study of sea-level change arising from GIA-induced perturbations in the Earth's rotation vector, both Han & Wahr (1989) and Bills & James (1996) (hereafter referred to as HW and BJ, respectively) included only the Laurentide ice mass component of the Late Pleistocene ice cover. It is therefore of interest to examine how predictions of the rotation-induced component of sea-level change are affected by adopting this simpler ice model. Fig. 10 shows our predictions of the rotation-induced component of the sea-level signal calculated using the complete global ice cover (circles) and using only the Laurentide component of the global ice model (squares). The discrepancy is small, indicating that GIA-induced polar wander is driven almost entirely by the growth and decay of the Laurentide ice sheet. This is due to the fact that the cryospheric mass flux in the eastern hemisphere (that is between 0 and 180° east longitude) during the last deglaciation contributed a J^{L}_{23} inertia component which was only ∼20 per cent of

GJI000 24/3/98 10:34:01 3B2 version 5.20
The Charlesworth Group, Huddersfield 01484 517077

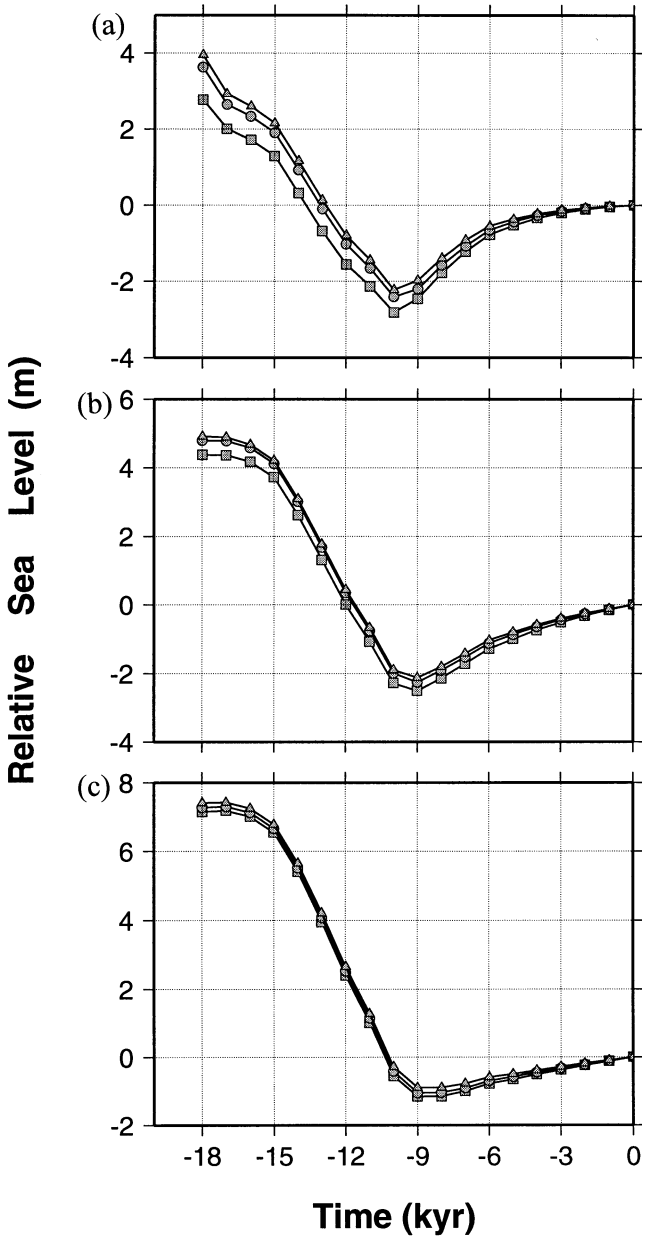

Figure 7. Predicted RSL change at Clinton (41.2N, −72.5E) due to variations in the rotation vector. Calculations are based on earth models with $\nu_{um} = 10^{21}$ Pa s and $\nu_{lm} = 10^{21}$ Pa s (a), 10^{22} Pa s (b) and 10^{23} Pa s (c). Within each frame, the curves correspond to calculations based on a lithospheric thickness of 70 km (squares), 120 km (circles) and 170 km (triangles).

the magnitude (and of opposite sign) to the contribution associated with the Laurentide ice complex. Thus, motion of the rotation pole along the x_2 axis (which dominates the calculated GIA-induced polar wander) is largely controlled by the growth and decay of the Laurentide ice sheet. Similar predictions for ν_{lm} ranging from 10^{21} to 10^{23} Pa s show that, in general, a maximum error of $\sim$10 per cent is introduced in predictions of the rotation-induced RSL signal when only the Laurentide ice mass is considered.

The dominance of the Laurentide ice sheet contribution to the rotation-induced RSL change raises an interesting issue. As discussed in the last section, the predicted RSL perturbation due to rotation is characterized by a transition from a phase of sea-level fall (rise) to a period of sea-level rise (fall) in quadrants associated with Australia and North America (South America and eastern Asia). The timing of this transition is linked to the end of the deglaciation event (and hence the end of the interval in which the direct effect of the rotational potential on sea level is significant). Although the ice model we have adopted (ICE-3G) is defined by a global deglaciation which ends at 5 kyr BP, the melting of the Laurentide ice sheet component of the model is essentially complete by 9 kyr BP (Tushingham & Peltier 1991). It is this specific aspect of the ice model which governs the timing of the sea-level transitions evident in Fig. 4.

HW presented predictions for a Maxwell viscoelastic earth model with $LT = 120$ km, and an isoviscous mantle of 10^{21} Pa s (see their Fig. 3). The temporal form of our rotation-induced RSL curves are significantly different from those shown in HW's Fig. 3. MM also recognized this discrepancy and argued that it resulted from the neglect, in HW, of the direct effect of the rotational potential. We explore this issue in Fig. 11, which shows the predicted rotation-induced RSL change (and its various contributions) at Clinton for the same earth model used by HW. (To be consistent with the HW predictions, the calculations in Fig. 11 do not include the influence of the rotation-induced water load and consider only the degree 2 order 1 component of the rotational potential.) Clearly, the direct effect of the rotational potential on sea level (squares) cannot be ignored since it is of an equal and opposite magnitude to the deformational effect (triangles); indeed, its omission leads to a significantly larger signal which lacks the important transition at $\sim$9 kyr BP.

As stated in the Introduction, BJ concluded that calculations based on a rigid earth model produce a reasonable first-order prediction of rotation-induced sea-level change. The sea-level response, for the case of a rigid earth model, is due solely to the direct effect of the rotational potential. It is clear from Fig. 11 that the direct effect cannot provide an accurate description of the total rotation-induced RSL response since LGM. As an example, a prediction based on the direct effect alone will not be characterized by the non-monotonicity evident in the total rotation-induced RSL response. Furthermore, the former calculation will yield an RSL amplitude that is significantly too large. BJ claim that the peak-to-peak amplitude of the total rotation-induced RSL signal reaches 40 m ($\pm$20 m). This is consistent with the 'direct effect' in Fig. 11; however, it is a factor of $\sim$5 larger than the actual rotation-induced signal.

The results in Fig. 11 also demonstrate why the BJ analysis led to predictions that are of opposite sign and comparable magnitude to those presented in HW (simply compare the squares and triangles in Fig. 11). As a specific example, Fig. 1 of BJ implies a fall in sea level over the deglaciation period at Clinton, while Fig. 3 of HW indicates a sea-level rise at this site.

We next consider the validity of several conclusions appearing in the BJ analysis. Inferences of mantle viscosity based on RSL predictions have commonly utilized data from the Hudson Bay region of north eastern Canada (e.g. Mitrovica & Peltier 1993; Han & Wahr 1995) and Australia (e.g. Nakada & Lambeck 1989). These are regions in which the polar-wander-induced sea-level change is near a maximum (Fig. 2) and this led BJ to state that '...failure to include it (the rotation-induced RSL contribution) in previous analyses of the sea-level

GJI000 24/3/98 10:34:13 3B2 version 5.20
The Charlesworth Group, Huddersfield 01484 517077

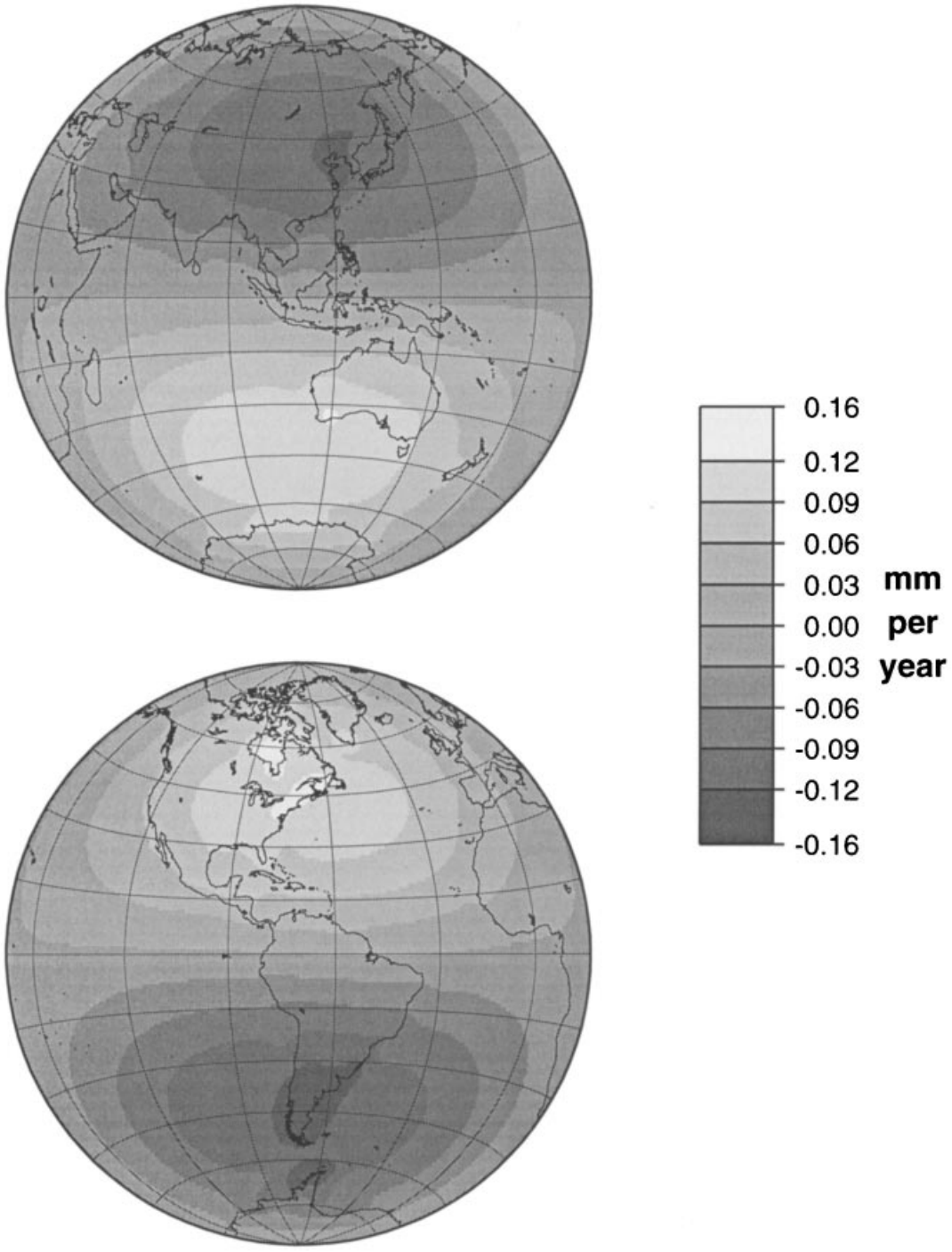

Figure 8. Present-day rates of sea-level change caused by GIA-induced perturbations to the rotation vector. Calculations are based on an earth model with $LT = 120$ km, $\nu_{um} = 10^{21}$ Pa s and $\nu_{lm} = 10^{22}$ Pa s. The signal is dominated by a degree 2 order 1 harmonic geometry with shorter-wavelength perturbations to this signal induced by the water load component associated with polar motion.

problem largely invalidates many ... quantitative inferences (of mantle viscosity)' (p. 3023). In Fig. 12 we show predictions of RSL variation at the Richmond Gulf site in Hudson Bay for the cases of a sea-level theory valid for a rotating and a non-rotating earth model and for two different viscosity profiles ($\nu_{lm} = 10^{21}$ or 10^{22} Pa s). It is clear, in contrast to the assertion by BJ, that the rotational RSL signal is far too small in magnitude to affect previous analyses using data from the Hudson Bay region of Canada. We note in this regard that the uncertainties in the observed RSL curves from this region (see e.g. Walcott 1972) are also significantly larger than the maximum predicted RSL contribution due to GIA-induced polar wander.

Next, we consider RSL predictions in the Australian region and its vicinity. Nakada & Lambeck (1989) used the difference in the measured Holocene highstands from five Australian sites

GJI000 24/3/98 10:34:25 3B2 version 5.20
The Charlesworth Group, Huddersfield 01484 517077

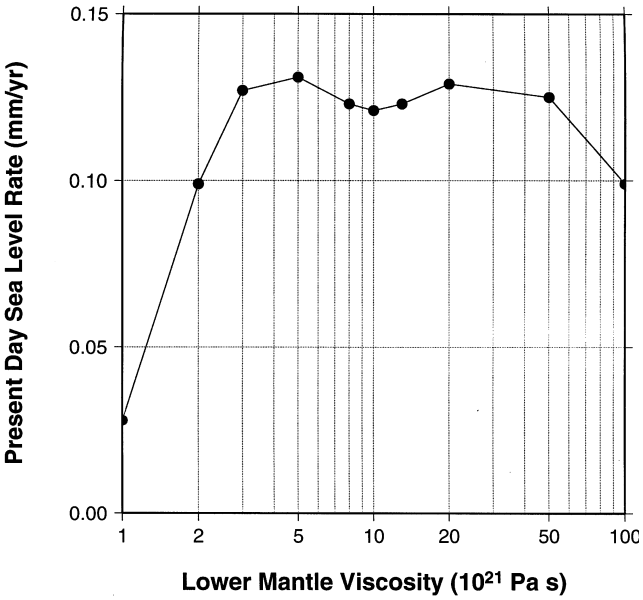

Figure 9. Predicted present-day sea-level-change rates due to polar wander at the site Clinton (41.2N, −72.5E) as a function of v_{lm}, for earth models characterized by $LT = 120$ km and $v_{um} = 10^{21}$ Pa s.

and one site in New Zealand to infer upper- and lower-mantle viscosity. In Table 1 we show predictions of differential sea-level highstands between sites considered by Nakada & Lambeck (1989) for the case of a sea-level theory appropriate to a rotating and a non-rotating Earth. As in Fig. 12, the calculations are based on earth models with $LT = 120$ km, $v_{um} = 10^{21}$ Pa s and either $v_{lm} = 10^{21}$ Pa s ('Viscosity Model 1') or 10^{22} Pa s ('Viscosity Model 2'). Since the rotation-induced sea-level geometry is dominated by a long-wavelength degree 2 spherical harmonic function, errors in differential sea-level highstands will be exceedingly small for sites in close proximity. From Table 1, the largest error incurred by neglecting the rotational contribution to the differential sea-level highstands is 0.2 m for the case of the Halifax Bay–Moruya and Moruya–Christchurch pairs. These errors will have no bearing on the viscosity inference based on these observables since the observational uncertainties are significantly larger than 0.2 m (see Table 1). The same conclusion holds for the other differential highstands considered in Table 1, and we conclude that the Nakada & Lambeck (1989) viscosity inferences (despite the assertions of BJ) would not be affected by the inclusion of Earth rotation in the GIA sea-level theory.

BJ also argue that the contribution of GIA-induced polar wander to sea-level change will probably bias previously constructed models of glacial loading and unloading based on RSL data (e.g. Tushingham & Peltier 1991; Peltier 1994). The RSL constraints adopted in Tushingham & Peltier (1991), for example, are generally younger than 10 kyr BP and were obtained from previously glaciated regions. Neglecting the rotational signal of RSL change would introduce a maximum error of ∼2 m over this time range (see Fig. 4). The RSL signals from previously glaciated regions and their associated error bars (e.g. Tushingham & Peltier 1991) are significantly larger than this signal and thus we conclude that inferences of the space–time geometry of the late Pleistocene ice loads will, in fact, be unaffected by the inclusion of a rotation-induced RSL signature.

Global models of late Pleistocene ice mass history have been tuned to match the eustatic sea-level history determined by Fairbanks (1989) on the basis of coral records from Barbados (e.g. Peltier 1994). Since the Barbados site is at low latitudes, the rotation-induced RSL signal will be small. In fact, the signal is roughly ∼3 m at 18 kyr BP in Fig. 2, which is consistently smaller (by a factor of 2–3) than the observational uncertainty in RSL data of this age. We conclude that the previously applied 'tuning' procedure remains valid (see also MM).

Although differential sea-level highstands are not significantly affected by the rotation-induced RSL signal (Table 1), this signal may be large enough to bias estimates of melting events since the end of the deglaciation period (∼5 kyr BP to present) which are based on highstands for specific sites (that is, not differential highstands). Nakada and Lambeck (1989) used their preferred viscosity model to predict the absolute value of the observed Late Holocene highstands. They found that their predictions were consistently too high (by as much as 2–3 m at some sites) and this led them to infer ongoing late Holocene melting from the Antarctic ice complex. Our results indicate that the inclusion of a rotation-induced sea-level signal will act to lower the predicted highstands in the Australian region relative to those based on a theory valid for a static Earth by, on average, 0.5 m (see the Perth site in Fig. 4b). Thus, the new sea-level theory described in this paper will, when applied to the Nakada & Lambeck (1989) analysis, lead to lower estimates of late Holocene melting from Antarctica.

To this point we have not focused on the normal-mode nature of the load and rotational responses associated with the GIA process (see e.g. eqs 1 and 2). A recent study by Mitrovica & Milne (1998) has shown that the M1 mode of relaxation plays an important role in predictions of present-day polar wander rate due to GIA for values of lower-mantle viscosity below ∼10^{22} Pa s. The M1 mode is associated with the buoyancy-induced stress field resulting from the deflection of

Table 1. Predictions of differential sea-level highstands.

Site pairs	Observational constraint (datum = ξ)	Viscosity Model 1:		Viscosity Model 2:	
		Rotating	Non-rotating	Rotating	Non-rotating
Karumba—Halifax Bay	$\xi \geq 1.0$ m	0.6 m	0.6 m	0.9 m	0.9 m
Port Pirie—Cape Spencer	$2.5 \text{ m} \leq \xi \leq 4.0$ m	1.2 m	1.1 m	1.6 m	1.5 m
Halifax Bay—Moruya	$0.0 \text{ m} \leq \xi \leq 1.5$ m	−0.1 m	−0.2 m	2.6 m	2.4 m
Moruya—Christchurch	$-0.5 \text{ m} \leq \xi \leq 1.0$ m	−1.1 m	−1.1 m	−0.1 m	0.1 m

GJI000 24/3/98 10:34:29 3B2 version 5.20
The Charlesworth Group, Huddersfield 01484 517077

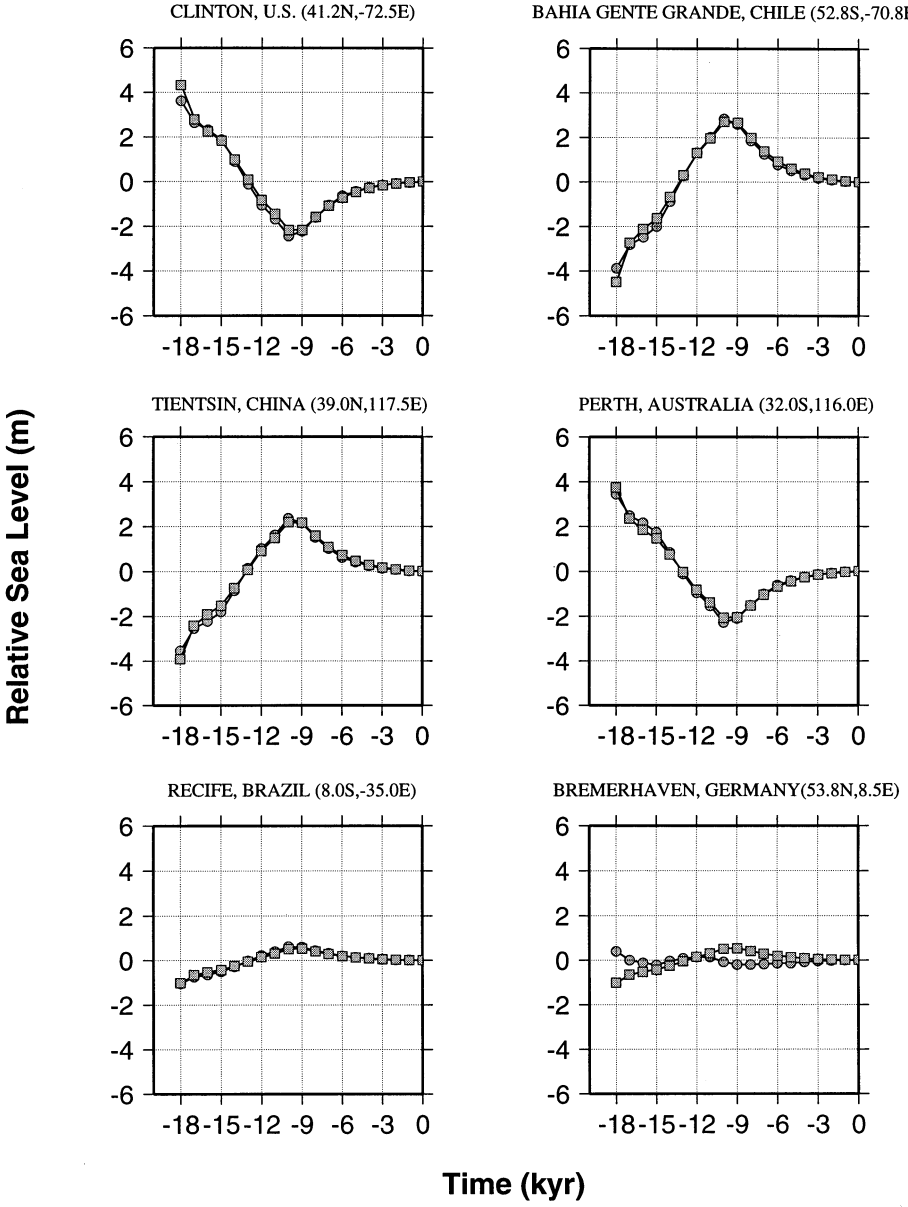

Figure 10. Rotation-induced RSL calculated using the global ICE-3G-based model (see text) (circles) and the Laurentide component of this model (squares). The earth model adopted in this calculation is characterized by a lithospheric thickness of 120 km and an isoviscous mantle of 10^{21} Pa s.

the density (seismic) discontinuity at 670 km depth. However, the mode will only contribute to the GIA process if the boundary behaves non-adiabatically on GIA timescales. Since this behaviour is a point of some contention (e.g. Fjeldskaar & Cathles 1984; Mitrovica & Peltier 1989) it is worthwhile determining how sensitive our predictions of polar-wander-induced sea-level change are to the existence of this relaxation mode. Fig. 13 shows the rotational component of sea-level change calculated for two earth models. These are characterized by $LT = 120$ km, $\nu_{\rm um} = 10^{21}$ Pa s and either $\nu_{\rm lm} = 10^{21}$ Pa s or $\nu_{\rm lm} = 10^{22}$ Pa s. For each model the signal is shown for the cases in which the M1 mode of relaxation is included or removed. [Note that we are investigating the effect of a perfectly adiabatic boundary at 670 km depth by simply removing the M1 mode calculated for an earth model which includes the seismically inferred density jump at this depth. This procedure, which has been adopted in several previous GIA analyses (e.g. Yuen *et al.* 1986; Mitrovica & Milne 1997), is, however, only an approximate treatment of this problem. The reader is referred to the recent work by Johnston, Lambeck & Wolf (1997) for a more rigorous approach.] The M1 mode has a relatively large effect in the case of the isoviscous model, producing a ~ 50 per cent reduction in the RSL signal over the last 18 kyr. In accord with the polar wander predictions of Mitrovica & Milne (1997), the effect of the M1 mode decreases monitonically as the value of $\nu_{\rm lm}$ is increased, and is only significant (discrepancy greater than ~ 20 per cent) for models with $\nu_{\rm lm}$ in the range $1\text{–}5 \times 10^{21}$ Pa s.

Figs 8 and 9 consider the effect of GIA-induced polar wander on predicted rates of present-day sea-level change.

GJI000 24/3/98 10:34:42 3B2 version 5.20
The Charlesworth Group, Huddersfield 01484 517077

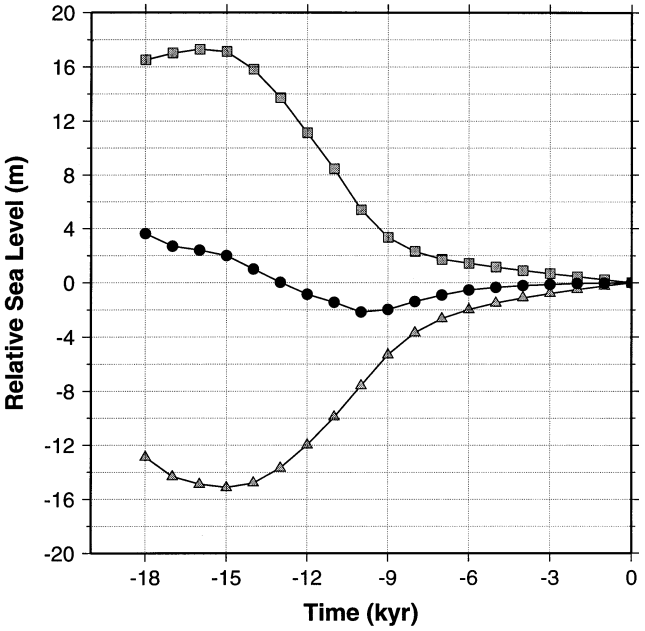

Figure 11. The predicted degree 2 order 1 component of sea-level change induced by the rotational potential for the site Clinton (41.2N, −72.5E) (the associated water loading effect has not been included). The squares denote the direct effect of the rotational potential on sea level while the triangles denote the viscoelastic sea-level response. The sum of these curves gives the total sea-level signal shown by the black circles. These calculations are based on an earth model with $LT = 120$ km and an isoviscous mantle of 10^{21} Pa s.

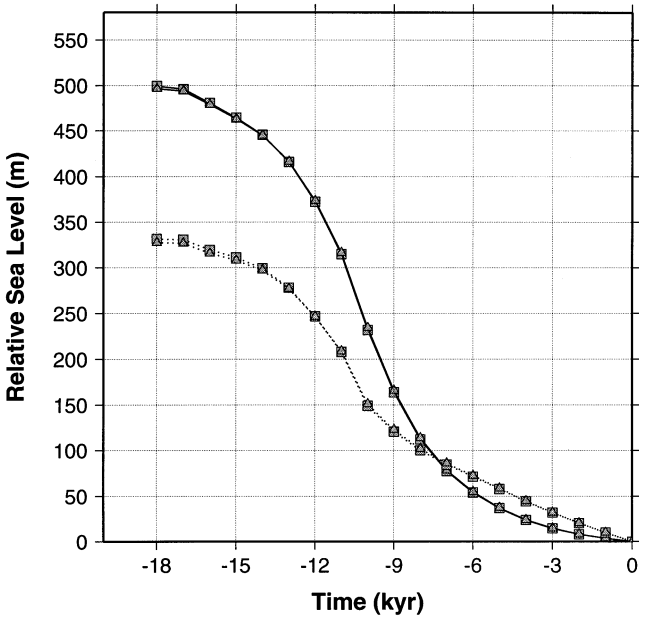

Figure 12. Predicted postglacial RSL curves at the site Richmond Gulf (57.0N, −77.0E) in northeastern Canada. The squares denote predictions based on the sea-level equation valid for a rotating Earth, while the triangles denote predictions based on the sea-level equation for a non-rotating Earth. The solid lines represent calculations that adopted an earth model with $LT = 120$ km and an isoviscous mantle of 10^{21} Pa s, whereas the dotted lines represent calculations that adopted the same earth model except that ν_{lm} was increased to 10^{22} Pa s.

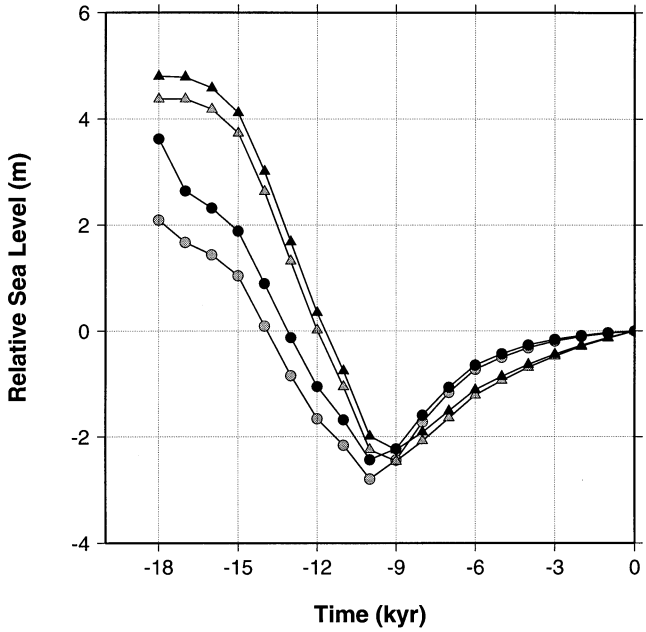

Figure 13. Predicted sea-level change produced by GIA-induced variations in the rotation vector for earth models with $LT = 120$ km lithosphere, $\nu_{um} = 10^{21}$ Pa s and either $\nu_{lm} = 10^{21}$ Pa s (black circles) or 10^{22} Pa s (black triangles). The curves denoted by shaded circles and triangles are analogous to those which adopt the black symbols with the exception that the M1 mode of relaxation has been removed.

The signal reaches a magnitude of ~ 0.15 mm yr^{-1} in certain locations (this predicted magnitude increases to ~ 0.17 mm yr^{-1} when a thin, ~ 70 km lithosphere is adopted). We conclude that previous analyses that have attempted to estimate global present-day sea-level change using tide gauge data sets may be slightly biased if a significant proportion of the data is obtained from regions in which the rotation-induced sea-level signal is large. For example, the present-day sea-level rise estimated by Davis & Mitrovica (1996) (1.5 ± 0.3 mm yr^{-1}) on the basis of tide gauge data from the east coast of North America is reduced by approximately 10 per cent by incorporating earth rotation into the sea-level theory (see also MM).

REFERENCES

Bills, B.G. & James, T.S., 1996. Late Quaternary variations in relative sea level due to glacial cycle polar wander, *Geophys. Res. Lett.,* **23,** 3023–3026.

Clark, J.A., Farrell, W.E. & Peltier, W.R., 1978. Global changes in postglacial sea level: a numerical calculation, *Quat. Res.,* **9,** 265–287.

Davis, J.L. & Mitrovica, J.X., 1996. Glacial isostatic adjustment and the anomalous tide gauge record of eastern North America, *Nature,* **379,** 331–333.

Dziewonski, A.M. & Anderson, D.L., 1981. Preliminary Reference Earth Model (PREM), *Phys. Earth planet. Inter.,* **25,** 297–356.

Fairbanks, R.G., 1989. A 17,000-year glacio-eustatic sea level record: influence of glacial melting rates on the Younger Dryas event and deep ocean circulation, *Nature,* **342,** 637–642.

Farrell, W.E. & Clark, J.A., 1976. On postglacial sea level, *Geophys. J. R. astr. Soc.,* **46,** 647–667.

Fjeldskaar, W. & Cathles, L.M., 1984. Measurement requirements for glacial uplift detection of nonadiabatic density gradients in the mantle, *J. geophys. Res.,* **89,** 10 115–10 124.

GJI000 24/3/98 10:34:47 3B2 version 5.20
The Charlesworth Group, Huddersfield 01484 517077

Han, D. & Wahr, J., 1989. Post-glacial rebound analysis for a rotating Earth, in *Slow Deformations and Transmission of Stress in the Earth,* pp. 1–6, eds Cohen, S. & Vanicek, P., *AGU Mono. Series 49*.

Han, D. & Wahr, J., 1995. The viscoelastic relaxation of a realistically stratified Earth, and a further analysis of postglacial rebound, *Geophys. J. Int.,* **120,** 287–311.

Heiskanen, W.A. & Moritz, H., 1967. *Physical Geodesy,* W. H. Freeman & Co., San Francisco, CA.

Johnston, P., 1993. The effect of spatially non-uniform water loads on predictions of sea level change, *Geophys. J. Int.,* **114,** 615–634.

Johnston, P., Lambeck, K. & Wolf, D., 1997. Material versus isobaric internal boundaries in the Earth and their influence on postglacial rebound, *Geophys. J. Int.,* **129,** 252–268.

Lambeck, K., 1980. *The Earth's Variable Rotation,* Cambridge University Press, Cambridge.

Lambeck, K., 1993. Glacial rebound of the British Isles—II. A high resolution, high-precision model, *Geophys. J. Int.,* **115,** 960–990.

Miller, S.P. & Wunsch, C., 1973. The pole tide, *Nature,* **246,** 98–102.

Milne, G.A. & Mitrovica, J.X., 1996. Postglacial sea-level change on a rotating Earth: first results from a gravitationally self-consistent sea-level equation, *Geophys. J. Int.,* **126,** F13–F20.

Mitrovica, J.X. & Milne, G.A., 1998. Glaciation-induced perturbations in the Earth's rotation: a new appraisal, *J. geophys. Res.,* **103,** 985–1005.

Mitrovica, J.X. & Peltier, W.R., 1989. Pleistocene deglaciation and the global gravity field, *J. geophys. Res.,* **94,** 13 651–13 671.

Mitrovica, J.X. & Peltier, W.R., 1991. On post-glacial geoid subsidence over the equatorial oceans, *J. geophys. Res.,* **96,** 20 053–20 071.

Mitrovica, J.X. & Peltier, W.R., 1993. A new formalism for inferring mantle viscosity based on estimates of post glacial decay times: Application to RSL variations in N.E. Hudson Bay, *Geophys. Res. Lett.,* **20,** 2183–2186.

Munk, W.H. & MacDonald, G.J.F., 1960. *The Rotation of the Earth,* Cambridge University Press, Cambridge.

Nakada, M. & Lambeck, K., 1989. Late Pleistocene and Holocene sea-level change in the Australian region and mantle rheology, *Geophys. J. Int.,* **96,** 497–517.

Peltier, W.R., 1974. The impulse response of a Maxwell Earth, *Rev. Geophys.,* **12,** 649–669.

Peltier, W.R., 1994. Ice age paleotopography, *Science,* **265,** 195–201.

Peltier, W.R. & Andrews, J.T., 1976. Glacial isostatic adjustment—I. The forward problem, *Geophys. J. R. astr. Soc.,* **46,** 605–646.

Peltier, W.R. & Tushingham, A.M., 1991. Influence of glacial isostatic adjustment on tide gauge measurements of secular sea level change, *J. geophys. Res.,* **96,** 6779–6796.

Sabadini, R., Yuen, D.A. & Boschi, E., 1982. Polar wander and the forced responses of a rotating, multilayered, viscoelastic planet, *J. geophys. Res.,* **87,** 2885–2903.

Sabadini, R., Doglioni, C. & Yuen, D.A., 1990. Eustatic sea level fluctuations induced by polar wander, *Nature,* **345,** 708–709.

Spada, G., Ricard, Y. & Sabadini, R., 1992. Excitation of true polar wander by subduction, *Nature,* **360,** 452–454.

Steinberger, B.M. & O'Connell, R.J., 1997. Change of the Earth's rotation axis inferred from advection of mantle density heterogeneities, *Nature,* **387,** 169–173.

Tushingham, A.M. & Peltier, W.R., 1991. ICE-3G: A new global model of late Pleistocene deglaciation based on geophysical predictions of post-glacial relative sea level change, *J. geophys. Res.,* **96,** 4497–4523.

Vermeersen, L.L.A. & Sabadini, R., 1996. Significance of the fundamental mantle relaxation mode in polar wander simulations, *Geophys. J. Int.,* **127,** F5–F9.

Wahr, J.M., 1985. Deformation induced by polar motion, *J. geophys. Res.,* **90,** 9363–9368.

Walcott, R.I., 1972. Quaternary vertical movements in eastern North America: Quantitative evidence of glacio-isostatic rebound, *Rev. Geophys. Space Phys.,* **10,** 849–884.

Wu, P. & Peltier, W.R., 1983. Glacial isostatic adjustment and the free air gravity anomaly as a constraint on deep mantle viscosity, *Geophys. J. R. astr. Soc.,* **74,** 377–449.

Wu, P. & Peltier, W.R., 1984. Pleistocene deglaciation and the Earth's rotation: A new analysis, *Geophys. J. R. astr. Soc.,* **76,** 753–792.

Yuen, D.A., Sabadini, R. & Boschi, E., 1982. Viscosity of the lower mantle as inferred from rotational data, *J. geophys. Res.,* **87,** 10 745–10 762.

Yuen, D.A., Sabadini, R., Gasperini, P. & Boschi, E., 1986. On transient rheology and glacial isostasy, *J. geophys. Res.,* **91,** 11 420–11 438.

GJI000 24/3/98 10:34:58 3B2 version 5.20
The Charlesworth Group, Huddersfield 01484 517077